

1 **Assessment of the SMAP Level-4 Surface and Root-Zone Soil Moisture Product Using *In***  
2 ***Situ* Measurements**

3  
4 Rolf H. Reichle<sup>1</sup>, Gabrielle J. M. De Lannoy<sup>2</sup>, Qing Liu<sup>1,3</sup>, Joseph V. Ardizzone<sup>1,3</sup>, Andreas  
5 Colliander<sup>4</sup>, Austin Conaty<sup>1,3</sup>, Wade Crow<sup>5</sup>, Thomas J. Jackson<sup>5</sup>, Lucas A. Jones<sup>6</sup>, John S.  
6 Kimball<sup>6</sup>, Randal D. Koster<sup>1</sup>, Sarith P. Mahanama<sup>1,3</sup>, Edmond B. Smith<sup>1,3</sup>, Aaron Berg<sup>7</sup>, Simone  
7 Bircher<sup>8</sup>, David Bosch<sup>9</sup>, Todd G. Caldwell<sup>10</sup>, Michael Cosh<sup>5</sup>, Ángel González-Zamora<sup>11</sup>,  
8 Chandra D. Holifield Collins<sup>12</sup>, Karsten H. Jensen<sup>13</sup>, Stan Livingston<sup>14</sup>, Ernesto Lopez-Baeza<sup>15</sup>,  
9 José Martínez-Fernández<sup>11</sup>, Heather McNairn<sup>16</sup>, Mahta Moghaddam<sup>17</sup>, Anna Pacheco<sup>16</sup>, Thierry  
10 Pellarin<sup>18</sup>, John Prueger<sup>19</sup>, Tracy Rowlandson<sup>7</sup>, Mark Seyfried<sup>20</sup>, Patrick Starks<sup>21</sup>, Zhongbo Su<sup>22</sup>,  
11 Marc Thibeault<sup>23</sup>, Rogier van der Velde<sup>22</sup>, Jeffrey Walker<sup>24</sup>, Xiaoling Wu<sup>24</sup>, and Yijian Zeng<sup>22</sup>

12  
13 *Journal of Hydrometeorology*

14  
15 *Submitted:* 7 Apr 2017

16 *Revised:* 10 Jul 2017

17  
18 <sup>1</sup>NASA Goddard Space Flight Center, Greenbelt, MD, USA

19 <sup>2</sup>KU Leuven, Heverlee, Belgium

20 <sup>3</sup>Science Systems and Applications, Inc., Lanham, MD, USA

21 <sup>4</sup>Jet Propulsion Laboratory, Pasadena, CA, USA

22 <sup>5</sup>USDA ARS Hydrology and Remote Sensing Laboratory, Beltsville, MD, USA

23 <sup>6</sup>University of Montana, Missoula, MT, USA

24 <sup>7</sup>Department of Geography, University of Guelph, Guelph, Ontario, Canada

25 <sup>8</sup>CESBIO, University of Toulouse, CNES/CNRS/IRD/UPS, Toulouse, France

26 <sup>9</sup>USDA ARS Southeast Watershed Research, Tifton, GA, USA

27 <sup>10</sup>Jackson School of Geosciences, University of Texas at Austin, Austin, TX, USA

28 <sup>11</sup>University of Salamanca, Villamayor, Spain

29 <sup>12</sup>USDA ARS Southwest Watershed Research Center, Tucson, AZ, USA

30 <sup>13</sup>Department of Geosciences and Natural Resource Management, University of Copenhagen,  
31 Copenhagen, Denmark

32 <sup>14</sup>USDA ARS National Soil Erosion Research Lab, West Lafayette, IN, USA

33 <sup>15</sup>University of Valencia, Valencia, Spain

34 <sup>16</sup>Agriculture and Agri-Food Canada, Ottawa, Ontario, Canada

35 <sup>17</sup>University of Southern California, Los Angeles, CA, USA

36 <sup>18</sup>University of Grenoble Alpes, CNRS, IRD, Grenoble INP, IGE, Grenoble, France

37 <sup>19</sup>USDA ARS National Laboratory for Agriculture and the Environment, Ames, IA, USA

38 <sup>20</sup>USDA ARS Northwest Watershed Research Center, Boise, ID, USA

39 <sup>21</sup>USDA ARS Grazinglands Research Laboratory, El Reno, OK, USA

40 <sup>22</sup>Faculty of Geo-Information Science and Earth Observations (ITC), University of Twente,  
41 Enschede, Netherlands

42 <sup>23</sup>Comisión Nacional de Actividades Espaciales, Buenos Aires, Argentina

43 <sup>24</sup>Monash University, Clayton, Victoria, Australia

44  
45 **Corresponding author address:**

46 Rolf H. Reichle

47 NASA Goddard Space Flight Center  
48 Global Modeling and Assimilation Office (Code 610.1)  
49 8800 Greenbelt Road  
50 Greenbelt, MD 20771  
51 USA  
52  
53 Tel.: 301-614-5693  
54 Email: [rolf.reichle@nasa.gov](mailto:rolf.reichle@nasa.gov)

55 **Abstract**

56 The Soil Moisture Active Passive (SMAP) mission Level-4 Surface and Root-Zone Soil  
57 Moisture (L4\_SM) data product is generated by assimilating SMAP L-band brightness  
58 temperature observations into the NASA Catchment land surface model. The L4\_SM product is  
59 available from 31 March 2015 to present (within 3 days from real-time) and provides 3-hourly,  
60 global, 9-km resolution estimates of surface (0-5 cm) and root-zone (0-100 cm) soil moisture and  
61 land surface conditions. This study presents an overview of the L4\_SM algorithm, validation  
62 approach, and product assessment versus *in situ* measurements. Core validation sites provide  
63 spatially averaged surface (root-zone) soil moisture measurements for 43 (17) “reference pixels”  
64 at 9-km and 36-km grid-cell scales located in 17 (7) distinct watersheds. Sparse networks  
65 provide point-scale measurements of surface (root-zone) soil moisture at 406 (311) locations.  
66 Core validation site results indicate that the L4\_SM product meets its soil moisture accuracy  
67 requirement, specified as an unbiased RMSE (ubRMSE, or standard deviation of the error) of  
68  $0.04 \text{ m}^3 \text{ m}^{-3}$  or better. The ubRMSE for L4\_SM surface (root-zone) soil moisture is  $0.038 \text{ m}^3 \text{ m}^{-3}$   
69 ( $0.030 \text{ m}^3 \text{ m}^{-3}$ ) at the 9-km scale and  $0.035 \text{ m}^3 \text{ m}^{-3}$  ( $0.026 \text{ m}^3 \text{ m}^{-3}$ ) at the 36-km scale. The  
70 L4\_SM estimates improve (significantly at the 5% level for surface soil moisture) over model-  
71 only estimates, which do not benefit from the assimilation of SMAP brightness temperature  
72 observations and have a 9-km surface (root-zone) ubRMSE of  $0.042 \text{ m}^3 \text{ m}^{-3}$  ( $0.032 \text{ m}^3 \text{ m}^{-3}$ ).  
73 Time series correlations exhibit similar relative performance. The sparse network results  
74 corroborate these findings over a greater variety of climate and land cover conditions.

75

76

77

78 **1. Introduction**

79 The Soil Moisture Active Passive (SMAP) mission has been providing global observations of L-  
80 band (1.4 GHz) passive microwave brightness temperature since 31 March 2015 at about 40-km  
81 resolution from a 685-km, near-polar, sun-synchronous orbit (Entekhabi et al. 2010a; Piepmeier  
82 et al. 2017). These observations are highly sensitive to surface soil moisture and temperature,  
83 which impact the land surface water and energy balance through, for example, the partitioning of  
84 rainfall into runoff and infiltration, and the partitioning of net radiation into latent and sensible  
85 heat fluxes. Thus, SMAP observations can be used to enhance our understanding of processes  
86 that link the water, energy, and nutrient cycles, and, ultimately, to extend the capabilities of  
87 current weather and climate prediction models (Entekhabi et al. 2014).

88

89 L-band brightness temperature observations and surface soil moisture retrievals similar to those  
90 from SMAP are also available from the Soil Moisture Ocean Salinity (SMOS) mission, launched  
91 in November 2009 (Kerr et al. 2010; De Lannoy et al. 2015). Moreover, surface soil moisture  
92 retrievals are available from a variety of past and current, active and passive satellite sensors,  
93 including the Advanced Microwave Scanning Radiometers (Mladenova et al. 2014; Parinussa et  
94 al. 2015) and the Advanced Scatterometer (Wagner et al. 2013). Because the latter instruments  
95 take measurements at C- and/or X-band (i.e., at frequencies higher than L-band), they provide  
96 observations that have slightly higher spatial resolution but are more sensitive to vegetation and  
97 thus less sensitive to soil conditions than SMOS and SMAP, resulting in noisier and less accurate  
98 soil moisture retrievals (Kerr et al. 2016). In addition to satellite retrievals, global soil moisture  
99 data are also available from reanalysis products (Saha et al. 2010; Dee et al. 2011; Gelaro et al.  
100 2017) and operational numerical weather prediction systems (de Rosnay et al. 2013; Lucchesi

101 2013a). Some of these model-based products assimilate surface observations to improve the  
102 quality of the soil moisture estimates. For example, the SM-DAS-2 product (Albergel et al.  
103 2012) assimilates ASCAT surface soil moisture retrievals and screen-level air temperature and  
104 humidity measurements. Furthermore, precipitation observations are used in several reanalysis  
105 products, including the Climate Forecasting System Reanalysis (Saha et al. 2010), MERRA-  
106 Land (Reichle et al. 2011), ERA-Interim/Land (Balsamo et al. 2015), and MERRA-2 (Reichle et  
107 al. 2017a,b).

108

109 The SMAP Level-4 Surface and Root-Zone Soil Moisture (L4\_SM) product is generated using a  
110 land data assimilation system that combines the advantages of space-borne L-band brightness  
111 temperature measurements, precipitation observations, and land surface modeling (section 2).  
112 The land model's key strength is its reliance on conservation principles for water (converting  
113 precipitation inputs into evaporation, runoff, and storage change) and energy (converting  
114 incident radiation into outgoing radiation, latent heat flux, sensible heat flux, storage change, and  
115 other miscellaneous terms). Given realistic forcing data, these conservation principles ensure at  
116 least some first-order reliability in the simulation products, which are then further corrected  
117 through the assimilation of SMAP brightness temperature observations.

118

119 The L4\_SM assimilation system provides two major and invaluable benefits for soil moisture  
120 estimation. First, the system facilitates complete coverage in space and time (as opposed to just  
121 the times and locations of satellite overpasses). Second, the embedded land model provides a  
122 means for producing soil moisture estimates at levels below the ~0-5 cm surface layer that is  
123 directly sampled by the satellite instrument. By design, the L4\_SM surface and deeper layer soil

124 moisture estimates are consistent with the available SMAP satellite observations. That is, during  
125 the course of the data assimilation process, the subsurface transport formulations in the land  
126 model (along with the subsurface assimilation updates) effectively propagate the surface soil  
127 moisture and temperature information that is contained in the SMAP brightness temperatures  
128 into the deeper soil levels. The L4\_SM product thus facilitates the use of SMAP data in  
129 applications that require complete spatio-temporal coverage and/or knowledge of deeper-layer  
130 soil moisture. The latter is particularly relevant for drought monitoring, water resource  
131 management, and sub-seasonal to seasonal climate forecasting.

132

133 The SMAP L4\_SM product is available every three hours on a global grid with 9-km spacing,  
134 thereby interpolating and extrapolating the coarser-scale (~40 km) SMAP observations in time  
135 and in space (both horizontally and vertically). The product is published within about 3 days  
136 from the time of observation, with the latency primarily dictated by the availability of the gauge-  
137 based precipitation product used to drive the land model (Reichle and Liu 2014).

138

139 The main objective of this study is to assess the quality of the L4\_SM soil moisture and  
140 temperature estimates versus *in situ* measurements. In the following, we describe the L4\_SM  
141 algorithm and product (section 2), discuss our validation approach (section 3), evaluate the  
142 L4\_SM product against *in situ* measurements (section 4), and provide a summary and  
143 conclusions (section 5). A companion paper (Reichle et al. 2017c) assesses the internal  
144 diagnostics of the L4\_SM algorithm, including the observation-minus-forecast residuals and the  
145 analysis increments. Their key findings, updated from (Reichle et al. 2016a), confirm that the

146 L4\_SM analysis is unbiased and produces realistic soil moisture and soil temperature increments  
147 that result in spatially consistent soil moisture and temperature analysis fields.

148

149

150

151

152

153

## 154 **2. L4\_SM Algorithm and Data Product**

155 Reichle et al. (2014) and De Lannoy and Reichle (2016a,b) provide a detailed description of the  
156 Goddard Earth Observing System, version 5 (GEOS-5), land data assimilation system (LDAS),  
157 which forms the basis of the L4\_SM algorithm. Here, we briefly summarize their discussion,  
158 highlight key features of the L4\_SM system, and point out differences between the L4\_SM  
159 algorithm and the SMOS assimilation described in (De Lannoy and Reichle 2016a,b).

160

### 161 *a. Overview*

162 The L4\_SM algorithm, shown schematically in Figure 1, is a customized version of the  
163 ensemble-based GEOS-5 LDAS built around the GEOS-5 Catchment Land Surface Model  
164 (hereinafter “Catchment model”; Koster et al. 2000; Ducharne et al. 2000). The primary drivers  
165 of this system are the SMAP L1C\_TB brightness temperature observations (section 2d) and the  
166 surface meteorological forcing data from the GEOS-5 atmospheric assimilation system,  
167 corrected with precipitation observations (section 2b). The SMAP brightness temperature  
168 observations are merged with the model estimates using a spatially distributed ensemble Kalman  
169 filter (EnKF; section 2d). Briefly, the L4\_SM algorithm interpolates and extrapolates the  
170 information from the SMAP observations and the model estimates in time and in space, taking  
171 into consideration the relative uncertainties of each; the L4\_SM data product represents the  
172 merged information.

173

174 The L4\_SM data are generated and distributed on the global, cylindrical, 9-km Equal-Area  
175 Scalable Earth, version 2 (EASEv2) grid (Brodzik et al. 2012). The L4\_SM outputs include soil  
176 moisture estimates for the “surface” (0-5 cm), “root-zone” (0-100 cm) and “profile” (0 cm to



177 depth of bedrock) layers. A single “root-zone” depth was chosen in the modeling system to  
178 make the SMAP product more straightforward; in nature, the depths tapped by roots vary with  
179 vegetation type, soil type, and other environmental factors (Jackson et al. 1996). Along with soil  
180 moisture, a large number of related land surface variables are also available in the L4\_SM  
181 product, including soil temperature, snow mass, land surface fluxes, surface meteorological  
182 forcing data, assimilation diagnostics, and land model parameters. L4\_SM surface soil  
183 temperature estimates are for the 0-10 cm layer except for tropical (broadleaf evergreen) forests,  
184 which are not considered here. The L4\_SM soil temperature and snow estimates can be used to  
185 screen or flag the L4\_SM soil moisture output for times and locations with frozen or snow-  
186 covered ground.

187

188 The generation of the L4\_SM product involves three basic time scales: (i) the land model  
189 computational time step of 7.5 min, (ii) the 3-hour EnKF analysis update time step, and (iii) the  
190 3-hour reporting (or output) time step for the published instantaneous and time-average output  
191 fields. The available SMAP brightness temperature observations are assimilated in an EnKF  
192 analysis update step at the nearest 3-hourly analysis time (0z, 3z, ..., and 21z). The latest  
193 L4\_SM data are generated operationally once per day by the NASA Global Modeling and  
194 Assimilation Office and then automatically delivered to the National Snow and Ice Data Center  
195 (NSIDC), where they become available to the public almost immediately.

196

197 Here, we use L4\_SM Version 2 data (Science Version ID: Vv2030) for the period from April  
198 2015 to November 2016. Specifically, we use 3-hourly, instantaneous “analysis” soil moisture  
199 and soil temperature fields from the “analysis update” files (Reichle et al. 2016b) and time-

200 invariant land model parameters (including soil porosity and wilting point) from the “land-  
201 model-constants” file (Reichle et al. 2016c). Note that 3-hourly time-average soil moisture and  
202 many other land surface fields are provided in the “geophysical” files (Reichle et al. 2016d). See  
203 (Reichle et al. 2015a) and the NSIDC website (<https://nsidc.org/data/smap/>) for complete lists of  
204 the available data fields and further details about data product specifications.

205

#### 206 *b. Modeling system*

207 In the Catchment model, the vertical character of soil moisture for each grid cell is determined (i)  
208 by the spatially varying equilibrium profile (defined by a balance of gravity and capillary forces)  
209 from the surface to the spatially (horizontally and vertically) varying water table (related to the  
210 model’s “*catchment deficit*” prognostic variable) and (ii) by two additional model prognostic  
211 variables that describe the average deviations from the equilibrium profiles in the 0-100 cm root-  
212 zone layer (“*root-zone excess*”) and in the 0-5 cm surface layer (“*surface excess*”). The  
213 volumetric soil moisture estimates provided in the L4\_SM product are diagnosed from these  
214 three model prognostic variables.

215

216 The Catchment model differs from traditional, layer-based models by including an explicit  
217 treatment of the spatial variation of soil water and water table depth within each 9-km grid cell  
218 based on the statistics of the catchment topography. This spatial variation enters into the  
219 calculation of moisture diffusion between the root-zone and deeper soil moisture storage. The  
220 treatment of spatial heterogeneity also allows for the diagnostic separation of each grid cell into  
221 “saturated”, “unsaturated”, and “wilting” sub-grid areas whose sizes vary dynamically. The  
222 surface energy balance is computed separately for each sub-grid area using physics specific to its

223 corresponding hydrological regime. For example, transpiration may be water-limited in the  
224 “unsaturated” sub-grid area while it is energy-limited in the “saturated” sub-grid area. This  
225 entails the monitoring of independent prognostic surface (“skin”) temperature variables for each  
226 sub-grid area, which in turn interact with an underlying, six-layer heat diffusion model for soil  
227 temperature that is common to all three sub-grid areas. A three-layer snow model component  
228 describes the state of the snow pack in terms of snow water equivalent, snow depth, and snow  
229 heat content (Stieglitz et al. 2001).

230

231 The Catchment model version and parameters of the (Version 2) L4\_SM system match those of  
232 MERRA-2 (Reichle et al. 2017b; their Table 2) except for the following four differences: (i) the  
233 L4\_SM soil hydraulic parameters are based on the pedotransfer functions of Wösten et al. (2001)  
234 applied to soil textures from the Harmonized World Soil Database (version 1.21) and the State  
235 Soil Geographic (STATSGO2) project (labeled “REV” in De Lannoy et al. 2014b); (ii) the  
236 WEMIN snow parameter, which governs the model’s snow depletion curve, is set to  $13 \text{ kg m}^{-2}$   
237 (Reichle et al. 2017b); (iii) the leaf area index is based on a merger of data from the Moderate-  
238 resolution Imaging Spectroradiometer (MODIS) and the GEOLAND product (Mahanama et al.  
239 2015); and (iv) the surface turbulence scheme is that of Louis (1979). For further details see De  
240 Lannoy and Reichle (2016a; their section 2b).

241

242 The observation-minus-forecast brightness temperature residuals needed in the soil moisture  
243 analysis (section 2d) are computed by converting the Catchment model soil moisture and  
244 temperature estimates into estimates of L-band brightness temperatures using a zero-order “tau-  
245 omega” radiative transfer model (RTM; De Lannoy et al. 2013). Select RTM input parameters,

246 including the microwave surface roughness, vegetation structure parameter, and scattering  
247 albedo, were calibrated prior to the SMAP launch using multi-angular L-band brightness  
248 temperature observations from SMOS (De Lannoy et al. 2014a). This calibration ensured that  
249 the long-term mean and variance of the modeled brightness temperatures match those of SMOS.  
250 Residual seasonal biases are addressed through rescaling (section 2d).

251  
252 The Catchment model is driven with surface meteorological forcing data from the GEOS-5  
253 forward-processing (FP) system at  $0.25^\circ \times 0.3125^\circ$  (latitude  $\times$  longitude) resolution (GEOS-5.13.0  
254 prior to 1 May 2015, then GEOS-5.13.1 until 24 January 2017, and GEOS-5.16 thereafter;  
255 Lucchesi 2013a). The GEOS-5 precipitation data are corrected with gauge-based precipitation  
256 observations from the NOAA Climate Prediction Center Unified (CPCU; Xie et al. 2007; Chen  
257 et al. 2008) product (Figure 1). The CPCU data are scaled to the climatology of the Global  
258 Precipitation Climatology Project, version 2.2 (GPCPv2.2; Adler et al. 2003; Huffman et al.  
259 2009) pentad precipitation product. The precipitation corrections are applied in full within  $42.5^\circ$   
260 latitude from the Equator except in Africa, where no corrections are applied because too few  
261 gauges are available there. Between  $42.5^\circ$  and  $62.5^\circ$  latitude (in the Northern and Southern  
262 Hemispheres), the precipitation corrections are linearly tapered between full corrections (at  $42.5^\circ$   
263 latitude) and no corrections (at  $62.5^\circ$  latitude). Poleward of  $62.5^\circ$  latitude, the model is forced  
264 with the uncorrected GEOS-5 FP precipitation. See Reichle and Liu (2014) and Reichle et al.  
265 (2017a) for further details on the precipitation correction algorithm.

266

267

268 *c. Nature Run (NRv4) simulation*

269 A longer-term, model-only simulation termed the Nature Run, version 4 (NRv4), was conducted  
270 for the period from 2001 through present. NRv4 is a single-member, unperturbed simulation  
271 using the Catchment model version of the L4\_SM algorithm on the same 9-km EASEv2 grid.  
272 Through 2013, the model is driven with surface meteorological forcing from the GEOS-5.9.1  
273 forward-processing for instrument teams (FP-IT) product at  $0.5^\circ \times 0.625^\circ$  (latitude  $\times$  longitude)  
274 resolution (Lucchesi 2013b). Thereafter, forcing is from the GEOS-5 FP product at  
275  $0.25^\circ \times 0.3125^\circ$  resolution (GEOS-5.11.0 prior to 1 Aug 2014, as for L4\_SM thereafter). The  
276 precipitation corrections used for NRv4 are the same as for the L4\_SM product.

277

278 The NRv4 simulation plays three roles in this study. First, the NRv4 simulation provides initial  
279 conditions for the ensemble simulation required to estimate the brightness temperature rescaling  
280 parameters, which in turn provides the ensemble initial conditions for the L4\_SM simulation  
281 starting 31 March 2015 at 0z. (NRv4 was itself spun up for 15 years.) Second, the NRv4  
282 simulation provides the multi-year climatological information needed to (i) calibrate the L4\_SM  
283 RTM parameters, (ii) determine the parameters that convert L4\_SM root-zone and profile soil  
284 moisture from volumetric to percentile units, and (iii) calibrate the Level-4 Carbon algorithm  
285 (Jones et al. 2017). Third, the NRv4 outputs provide a model-only reference skill against which  
286 the impact of the SMAP observations on the skill of the L4\_SM product can be measured  
287 (section 4).

288

289

290 *d. Assimilation of SMAP brightness temperature observations*

291 The Version 2 L4\_SM algorithm assimilates horizontally (H) and vertically (V) polarized SMAP  
292 brightness temperature observations from the Version 3 SMAP L1C\_TB product (Chan et al.  
293 2016a) after averaging the fore- and aft-looking measurements provided in the L1C\_TB product  
294 on their native 36-km EASEv2 grid. Brightness temperatures from the ascending (~6pm Equator  
295 crossing) and descending (~6am Equator crossing) half-orbits are assimilated. The Version 2  
296 L4\_SM algorithm does not assimilate data products that are based on the SMAP radar, which  
297 failed on 7 July 2015.

298

299 The ensemble-based L4\_SM data assimilation algorithm is shown schematically in Figure 1 of  
300 De Lannoy and Reichle (2016b), but note that for the L4\_SM system discussed here the model is  
301 on the 9-km grid and the assimilated SMAP observations are only available for a single, 40°  
302 incidence angle. The EnKF updates in the L4\_SM algorithm are spatially distributed in the sense  
303 that all observations within a radius of 1.25° impact the analysis at a given 9-km grid cell (De  
304 Lannoy and Reichle 2016b; their section 3.1). The weight of an observation-minus-forecast  
305 residual towards the soil moisture (and temperature) increments at a given 9-km grid cell is  
306 proportional to the modeled error correlations between the brightness temperature at the  
307 observation location and the soil moisture (and temperature) at the location of the increment.  
308 This correlation-based weight typically decays with increasing distance of the observation from  
309 the location of the increment. The L4\_SM system uses 24 ensemble members. The perturbation  
310 parameters for the model forcing and prognostic variables match those of De Lannoy and  
311 Reichle (2016a; their Table 2) except that the spatial correlation scale for the model prognostics  
312 perturbations is set to 0.3° in the L4\_SM system.

313  
314 Seasonally varying bias in the modeled brightness temperatures is addressed prior to assimilation  
315 by converting the observations and model forecast brightness temperatures into anomalies from  
316 their respective long-term mean seasonal cycles. Since the brightness temperature is strongly  
317 impacted by the surface temperature and the RTM parameters, this is done separately for each  
318 36-km grid cell, polarization, and orbit direction (i.e., time-of-day). For details, see De Lannoy  
319 and Reichle (2016a; their section 3b and Figures 1 and 2). For the Version 2 L4\_SM system, the  
320 mean seasonal cycles for the assimilated SMAP brightness temperatures were estimated from  
321 SMOS (version 5) observations for the period July 2010 to June 2014, after interpolating the  
322 SMOS data to the 40° SMAP incidence angle (De Lannoy et al. 2015). The mean seasonal  
323 cycles for the modeled brightness temperatures were computed from sub-sampled model output  
324 (at the times and locations of SMOS overpasses), generated with the ensemble L4\_SM modeling  
325 system using surface meteorological forcing as for NRv4 (section 2c).

326  
327 Only SMAP brightness temperature observations deemed to be of good quality are assimilated  
328 (that is, the lowest bit of the LIC\_TB quality flag must equal zero). Moreover, observations that  
329 fall outside the natural range between 100 K and 320 K are excluded from the assimilation.  
330 Observations are further screened based on the modeled soil temperature (must be greater than  
331 273.35 K) and snow mass (must be less than  $10^{-4}$  kg m<sup>-2</sup>) to exclude times and locations with  
332 frozen or snow-covered soil conditions, for which the RTM is not valid. Finally, the (hourly)  
333 precipitation rate at the observation time and location must be less than 2 mm h<sup>-1</sup> to minimize the  
334 detrimental impact of standing water on the analysis. These model-based conditions must be  
335 satisfied for all 9-km grid cells within a radius of 40 km from the center point of the observation.

336  
337  
338  
339  
340  
341  
342  
343  
344  
345  
346  
347  
348  
349  
350  
351  
352  
353  
354  
355  
356  
357  
358

The total brightness temperature observation error standard deviation is set to a constant value of 4 K. This error includes the instrument error (~1.3 K; Piepmeier et al. 2017) and the much larger representativeness error (~3.8 K). The latter consists of all errors associated with the observation operator, including errors in the approximation of the footprint of the satellite observations as well as errors in the RTM-based conversion of the model state vector into brightness temperatures. Since for a given brightness temperature observation only about 50 percent of the signal originates from a circle with a radius of 20 km, we assume an isotropic spatial correlation length for the observation error of  $0.25^\circ$ . Observation errors of H- and V-polarization brightness temperatures are assumed to be uncorrelated, even though this assumption is likely wrong for the representativeness error component. The estimates for the observation and model error parameters used in the L4\_SM system are similar to those of De Lannoy and Reichle (2016a,b) and are motivated by the positive results obtained with the assimilation of SMOS observations. Results presented below demonstrate that the assimilation of SMAP data with these error settings also produces skill enhancements. Further refinement of the error parameters may lead to additional skill improvements but is left for future work.



359 **3. Validation Approach and Measurements**

360 The L4\_SM product is primarily validated through comparison with independent *in situ*  
361 measurements (section 4). Suitable measurements fall into two main categories: (i) For a limited  
362 set of climate and land cover conditions, “core validation site” measurements provide accurate  
363 estimates of soil moisture at the 9-km or 36-km scales of the model and satellite estimates  
364 (section 3b). (ii) For a much wider range of conditions, “sparse network” measurements provide  
365 soil moisture estimates at a single, point-scale location within a 9-km model grid cell (section  
366 3c).

367

368 *a. L4\_SM accuracy requirement, validation metrics, and processing of in situ measurements*

369 The accuracy requirement for the L4\_SM surface and root-zone soil moisture estimates is that  
370 their average unbiased RMSE (ubRMSE) versus *in situ* measurements must be less than  $0.04 \text{ m}^3$   
371  $\text{m}^{-3}$  (excluding regions of snow and ice, frozen ground, mountainous topography, open water,  
372 urban areas, and vegetation with water content greater than  $5 \text{ kg m}^{-2}$ ). The ubRMSE is the  
373 RMSE computed after removing the long-term mean bias from the data, also referred to as the  
374 standard deviation of the error (Entekhabi et al. 2010b; Reichle et al. 2015b, their Appendix A).  
375 The meeting of the requirement is verified by comparing the L4\_SM estimates to the 9-km grid-  
376 cell scale *in situ* measurements from the core validation sites (section 3b).

377

378 In addition to the ubRMSE, we also determine the time series correlation coefficient R and the  
379 bias. The latter is computed as the mean of the differences between the L4\_SM (or NRv4)  
380 estimates and the *in situ* measurements (that is, estimates minus measurements). Metrics are  
381 computed wherever suitable *in situ* measurements are available, including for densely vegetated

382 or topographically complex areas outside of the limited geographic region for which the 0.04 m<sup>3</sup>  
383 m<sup>-3</sup> validation criterion applies. Metrics are computed using 3-hourly data for the period 1 April  
384 2015 to 31 March 2017 if at least 480 data points are available. All *in situ* measurements used  
385 here are subjected to extensive automated and manual quality control procedures following Liu  
386 et al. (2011), De Lannoy et al. (2014b), Entekhabi et al. (2014), and Reichle et al. (2015b; their  
387 Appendix C) to remove spikes, temporal inhomogeneities, oscillations, and other artifacts  
388 commonly seen in automated measurements. Moreover, we exclude times when the soil  
389 temperature is below 4°C or when the soil is partially or fully snow covered.

390

391 Surface soil moisture and temperature are validated against measurements from the uppermost  
392 sensor (typically at ~5 cm depth, see below). Root-zone soil moisture is validated against  
393 vertical averages of *in situ* measurements using weights that are proportional to the spacing of  
394 the sensor depths within the 0-100 cm layer (see below). In all cases, the deepest sensors used  
395 here are weighted most strongly. Vertical averages are only computed if all sensors within a  
396 given profile provide measurements that pass quality control.

397

398 For each statistic, we also computed 95% confidence intervals that take into account temporal  
399 autocorrelation in the time series (De Lannoy and Reichle 2016a; their section 4b). The metrics  
400 provided here are conservative skill estimates because they ignore errors in the *in situ*  
401 measurements. Triple Collocation techniques could be used to correct for such errors (Chen et  
402 al. 2017) but are not considered here. In any case, the *relative* performance of the L4\_SM and  
403 NRv4 estimates does not depend on the use of Triple Collocation approaches.

404

405

406 *b. Core validation site measurements*

407 Core validation sites have locally dense sensor networks that provide accurate soil moisture and  
408 soil temperature measurements at the grid-cell scale of the L4\_SM product. For any given core  
409 validation site, however, the spatial distribution of the *in situ* sensors is typically not aligned with  
410 the grid cells of the standard EASEv2 grid. Therefore, we defined custom “shifted” grid cells (or  
411 “reference pixels”) that better exploit the spatial coverage of the *in situ* measurements at each  
412 site, but that do not necessarily align with the standard EASEv2 grid (for examples, see Figure 4  
413 of Colliander et al. 2017). The grid-cell scale measurements are then computed as the weighted  
414 average of the contributing sensor measurements using Thiessen polygons or, if available,  
415 custom upscaling functions derived from intensive field campaigns (Colliander et al. 2017; their  
416 Figure 7).

417

418 A core validation site may provide *in situ* measurements for one or more 9-km and/or 36-km  
419 reference pixels. Core validation site reference pixels must satisfy a number of criteria,  
420 including verification through an intensive field campaign and provision of a minimum number  
421 and representative distribution of sensors within the reference pixel (Reichle et al. 2015b, their  
422 section 6.2; Colliander et al. 2017). For the comparison against the *in situ* measurements, the 9-  
423 km L4\_SM estimates are interpolated bi-linearly to the location of the 9-km reference pixels and  
424 are aggregated (using area-weighted averaging) for comparison to the 36-km reference pixel  
425 estimates. A repeat of the assessment using nearest-neighbor interpolation resulted in skill  
426 differences that were much smaller than the typical differences between the L4\_SM and NRv4  
427 skill metrics (not shown).

428

429 Table 1 lists the core validation sites and reference pixels used here consisting of a total of 43  
430 reference pixels from 19 different core validation sites. Table 2 breaks down the number of core  
431 validation sites and reference pixels with suitable quantities of measurements by variable and by  
432 horizontal scale. Surface soil moisture measurements are available for all 43 reference pixels.  
433 Root-zone soil moisture measurements are available for only 17 reference pixels. Root-zone soil  
434 moisture measurements at the 9-km scale are available from only 6 different sites, all of which  
435 are in North America (Little Washita, Fort Cobb, Little River, South Fork, Kenaston, and  
436 TxSON). Surface soil temperature measurements at 6am (6pm) are available for 35 (36)  
437 reference pixels. Average metrics across all reference pixels of a given horizontal scale (9-km  
438 or 36-km) are computed using the arithmetic average of the metrics at the individual reference  
439 pixels. The 95% confidence intervals are first averaged in the same way and then divided by the  
440 square root of the number of different core validation sites contributing to the metric (as listed in  
441 Table 2).

442  
443 Table 1 also lists the depths of the shallowest sensors, which are used to validate the L4\_SM  
444 surface soil moisture and surface soil temperature estimates. Moreover, Table 1 provides the  
445 depths of the deepest sensors that contribute to the *in situ* root-zone soil moisture measurements.  
446 At all reference pixels except Little River and Yanco, the deepest sensors are at 45 cm or 50 cm  
447 depth. At Little River, the deepest sensors are at 30 cm depth. At Yanco, the deepest sensors are  
448 installed vertically and centered at depths of 45 cm and 75 cm, representing the 30-60 cm and  
449 60-90 cm layers, respectively. For many sites, individual sensors tend to drop out temporarily,  
450 which leads to undesirable discontinuities in the reference pixel average soil moisture. To  
451 mitigate this effect, we require at least 8 individual, complete sensor profiles (after quality

452 control) to compute the reference pixel average, provided at least 8 sensor profiles were in the  
453 ground. For the 17 reference pixels that are based on fewer than 8 sensor profiles, we require  
454 data from all contributing sensor profiles (after quality control) to compute the reference pixel  
455 average. The time-average number of individual sensors that contribute to any given 36-km  
456 reference pixel average ranges between 6 and 33.2 for surface soil moisture (Table 1), with a  
457 mean value of 15.3 (not shown). At the 9-km scale, 14 of the 26 surface reference pixels are  
458 based on fewer than 8 individual sensor profiles, while the rest of the 9-km reference pixels have  
459 8 or more sensor profiles each (Table 1), with a mean value of 7.4 across all 9-km reference  
460 pixels (not shown).

461

#### 462 *c. Sparse network measurements*

463 The defining feature of sparse network measurements is that there is usually just one sensor (or  
464 profile of sensors) located within a given 9-km EASEv2 grid cell. The sparse network  
465 measurements used here include data from the USDA Natural Resources Conservation Service  
466 Soil Climate Analysis Network (SCAN; Schaefer et al. 2007), the US Climate Reference  
467 Network (USCRN; Bell et al. 2013; Diamond et al. 2013), the Oklahoma Mesonet (McPherson  
468 et al. 2007), and the OzNet in Australia's Murrumbidgee catchment (Smith et al. 2012). Note  
469 that for the Australian data, the core validation site and the sparse network results are not  
470 independent because about three quarters of the OzNet sites also contributed to the grid-cell scale  
471 soil moisture measurements of the Yanco reference pixels.

472

473 Table 3 lists the number of sparse network sites with sufficient data after quality control. Across  
474 all networks, 406 locations have surface and 311 have root-zone soil moisture measurements.

475 Most of the sites are in the continental United States, including about 100 each in the USCRN  
476 and SCAN networks, and another 100 in Oklahoma from the Mesonet. OzNet contributes 42  
477 sites with surface soil moisture measurements, 18 of which also provide root-zone  
478 measurements. Moreover, Table 3 lists the measurement depths used for computing root-zone  
479 measurements. For SCAN and USCRN sites, measurements at 50 cm (and occasionally 100 cm)  
480 depth are available. It is, however, very difficult to take and verify such deeper layer  
481 measurements consistently over long periods of time. These measurements are therefore not of  
482 the quantity and quality required for L4\_SM validation and are not used here. For OzNet, the  
483 measurements at the 45 cm depth are used as root-zone measurements.

484

485 The sparse network measurements are compared to the L4\_SM and NRv4 data from the standard  
486 9-km EASEv2 grid cell that includes the sensor location. Spatially averaged skill metrics are  
487 calculated by clustering sites geographically to keep densely sampled areas from dominating the  
488 validation metrics and to ensure realistic confidence intervals (De Lannoy and Reichle 2016a).  
489 The number of clusters is estimated a priori after prescribing an average cluster radius of  $1.5^\circ$ ,  
490 which is similar to the  $1.25^\circ$  compact support length scale of the L4\_SM analysis (section 2d).  
491 The 95% confidence intervals are first averaged in the same way and then divided by the square  
492 root of the number of clusters.

493

494 Sparse network results are grouped into locations with “favorable” or “unfavorable” conditions  
495 for soil moisture estimation from space-borne brightness temperature observations. Favorable  
496 locations include all areas where the accuracy requirement (section 3a) applies. Unfavorable  
497 locations include areas where (i) the maximum climatological leaf area index exceeds  $5 \text{ m}^2 \text{ m}^{-2}$

498 (MODIS 2008), (ii) the predominant land cover is forest, wetland, or urban according to the  
499 International Geosphere-Biosphere Programme (IGBP) DISCover (Loveland et al. 2000)  
500 vegetation classification, (iii) the topography is complex (elevation standard deviation greater  
501 than 71 m), or (iv) the elevation of the sensor location differs by more than 500 m from the mean  
502 elevation of the surrounding 36-km grid cell. The above grouping is determined using the land  
503 cover, vegetation, and topography parameters of the L4\_SM modeling system (Mahanama et al.  
504 2015).

505

506

507 **4. Results**

508 In this section, we present a detailed, quantitative analysis of the skill of the L4\_SM soil  
509 moisture and temperature estimates in reproducing *in situ* measurements from the core validation  
510 sites (section 4a) and sparse networks (section 4b). Some of the text in this section is from two  
511 non-peer reviewed project reports (Reichle et al. 2015b, 2016a) and has been updated to reflect  
512 the results obtained for the Version 2 L4\_SM product and the longer validation period used here.

513

514 *a. Core site validation*

515 In this subsection, we present the validation results using core site measurements. We first  
516 discuss the soil moisture validation results for three representative reference pixels (Little  
517 Washita, Little River, and South Fork) that exemplify features of the L4\_SM estimates and  
518 indicate aspects needing improvement. For reference, Table 4 lists the metrics for all 43  
519 reference pixels. Thereafter, we present average soil moisture and temperature metrics across all  
520 reference pixels and demonstrate that the L4\_SM product meets its accuracy requirement.

521

522 1) LITTLE WASHITA (OKLAHOMA)

523 The Little Washita, Oklahoma, site is situated in grasslands in a temperate, sub-humid climate.  
524 Based on several field campaigns that addressed *in situ* sensor calibration and upscaling (Cosh et  
525 al. 2006), the confidence in the quality of the *in situ* estimates at this site is very high, and good  
526 product performance at this site is considered to be important. Figure 2 shows the L4\_SM,  
527 NRv4, and *in situ* time series for the 36-km reference pixel. (The results for the 9-km reference  
528 pixel at Little Washita are qualitatively similar, but there are long gaps in the *in situ*  
529 measurements.) Soil moisture varies considerably during the validation period, owing to the



530 exceptionally wet conditions during May 2015 and the very dry conditions in August and  
531 September of both years. The L4\_SM and NRv4 estimates clearly capture the overall variability,  
532 as well as the timing of the major rainstorms. However, neither the NRv4 nor the L4\_SM  
533 estimates fully capture the wet conditions starting in late October 2015 and lasting through the  
534 winter of 2015-2016. Nevertheless, the time series correlation coefficients are very high, with R  
535 values of 0.81 for L4\_SM surface soil moisture and 0.88 for L4\_SM root-zone soil moisture,  
536 which is an improvement over the already high values of 0.73 and 0.87 for NRv4 surface and  
537 root-zone soil moisture, respectively (Table 4).

538  
539 The improvement is also reflected in the ubRMSE metric, which decreases from  $0.037 \text{ m}^3 \text{ m}^{-3}$  for  
540 NRv4 surface soil moisture to  $0.033 \text{ m}^3 \text{ m}^{-3}$  for L4\_SM, and from  $0.029 \text{ m}^3 \text{ m}^{-3}$  for NRv4 root-  
541 zone soil moisture to  $0.024 \text{ m}^3 \text{ m}^{-3}$  for L4\_SM (Table 4). The improvements are mostly due to  
542 the increased dynamic range and the generally faster dry-downs of the L4\_SM estimates  
543 resulting from the assimilation of the SMAP observations, which leads to a better match of the  
544 dry-downs indicated by the *in situ* measurements. Bias values are very low for surface soil  
545 moisture (around  $-0.01 \text{ m}^3 \text{ m}^{-3}$  for L4\_SM and NRv4). Root-zone soil moisture, however, is  
546 generally too dry and somewhat more biased for L4\_SM ( $-0.043 \text{ m}^3 \text{ m}^{-3}$ ) than for NRv4 ( $-0.037$   
547  $\text{m}^3 \text{ m}^{-3}$ ).

548  
549 2) LITTLE RIVER (GEORGIA)

550 The Little River, Georgia, site is in a humid agricultural environment, includes a substantial  
551 amount of tree cover, and has sandy soils. The site is also subject to irrigation and located near  
552 ephemeral, forested wetlands that can flood following rain events, but neither irrigation nor

553 wetland processes are considered in the L4\_SM modeling system. As for the Little Washita site,  
554 we show time series for the 36-km reference pixel at Little River (Figure 3) because of gaps in  
555 the *in situ* measurements at the 9-km reference pixel. All time series reflect a drop from  
556 somewhat wetter conditions in April and May of both years to drier summer conditions, with  
557 frequent yet typically modest rain events (Figure 3). The frequent wetting and drying events  
558 shown in the *in situ* measurements are reasonably captured by the L4\_SM and NRv4 estimates,  
559 but the exact timing and magnitude of the storms and dry-downs is less certain. Moreover, the  
560 tree cover, sandy soils, and irrigation at Little River complicate the modeling of soil moisture  
561 and brightness temperature, resulting in overall slightly lower skill values than for Little  
562 Washita.

563  
564 Despite the above complications, NRv4 estimates have reasonable skill, and the assimilation of  
565 SMAP observations again results in skill improvement. Surface soil moisture has an R value of  
566 0.68 for NRv4, which improves to 0.76 for L4\_SM. The correlation for root-zone soil moisture  
567 is higher, with R values of 0.81 for NRv4 and 0.84 for L4\_SM (Table 4). The assimilation also  
568 improves the ubRMSE values for surface soil moisture estimates from  $0.044 \text{ m}^3 \text{ m}^{-3}$  for NRv4 to  
569  $0.035 \text{ m}^3 \text{ m}^{-3}$  for L4\_SM and for root-zone soil moisture estimates from  $0.033 \text{ m}^3 \text{ m}^{-3}$  for NRv4  
570 to  $0.025 \text{ m}^3 \text{ m}^{-3}$  for L4\_SM. Bias values are relatively high at  $\sim 0.10 \text{ m}^3 \text{ m}^{-3}$  for surface soil  
571 moisture and  $\sim 0.07 \text{ m}^3 \text{ m}^{-3}$  for root-zone soil moisture. The SMAP and SMOS passive soil  
572 moisture retrievals also exhibit a wet bias (Chan et al. 2016b), which may be related to the  
573 ephemeral wetlands in the vicinity of the site. The wet bias in the NRv4 estimates, however,  
574 suggests that errors in the Catchment model parameters are the main reason for the wet bias in  
575 L4\_SM.

576

577 Figure 3 also reveals residual minor issues with the *in situ* measurements. Between May 17 and  
578 June 5, 2015, for example, the reference pixel average root-zone soil moisture shows somewhat  
579 erratic behavior. In this particular case, bad data from one sensor passed the automated quality  
580 control, and sensors also dropped out repeatedly during the period in question. The impact of  
581 these residual issues are very minor and do not impact our main conclusions.

582

### 583 3) SOUTH FORK (IOWA)

584 South Fork, Iowa, is in a cold climate agricultural region dominated by summer crops of corn  
585 and soybeans. Conditions in winter are mostly bare soil or stubble, followed by intensive tillage  
586 in early April that creates large surface roughness, which subsequently decreases again with  
587 additional soil treatments and rainfall, and as crops begin to cover the surface. Such variations in  
588 surface roughness are difficult to capture in the (climatological) microwave RTM parameters of  
589 the L4\_SM algorithm and in soil moisture retrieval algorithms in general (Patton and Hornbuckle  
590 2013). Moreover, at the 9-km and 36-km scales considered here, the land cover is a mix of corn  
591 and soybeans, which usually rotate each year, although there has been a trend toward more corn  
592 in recent years. By early July, for example, corn typically has a high vegetation water content of  
593  $\sim 3 \text{ kg m}^{-2}$  while that of soybeans is typically much smaller (around  $0.3 \text{ kg m}^{-2}$ ) (Jackson et al.  
594 2004). Finally, owing to the high clay content of the soils in this region, the agricultural fields  
595 are equipped with tiles to improve drainage. This local feature is not captured in the global-scale  
596 Catchment model of the L4\_SM algorithm.

597

598 Figure 4 shows soil moisture time series for a 9-km reference pixel at South Fork. Soil moisture  
599 conditions during the warm season are dominated by approximately weekly rain events with  
600 subsequent dry-downs. The L4\_SM surface soil moisture estimates capture this pattern and  
601 present a clear improvement over NRv4, especially in 2016. This is reflected in the ubRMSE  
602 values, which decrease from  $0.070 \text{ m}^3 \text{ m}^{-3}$  for NRv4 to  $0.053 \text{ m}^3 \text{ m}^{-3}$  for L4\_SM (Table 4). The  
603 surface soil moisture R value increases considerably from 0.08 for NRv4 to 0.62 for L4\_SM.  
604 Root-zone metrics show similar improvements for L4\_SM over NRv4, with ubRMSE values  
605 decreasing from  $0.044 \text{ m}^3 \text{ m}^{-3}$  for NRv4 to  $0.031 \text{ m}^3 \text{ m}^{-3}$  for L4\_SM and R values increasing  
606 considerably from 0.03 for NRv4 to 0.58 for L4\_SM. Generally, however, the L4\_SM estimates,  
607 and even more so the NRv4 estimates, do not capture the larger dynamic range of the *in situ*  
608 observations, which may be a reflection of the tile drainage. Bias values range from  $0.075 \text{ m}^3$   
609  $\text{m}^{-3}$  for NRv4 surface soil moisture to  $-0.014 \text{ m}^3 \text{ m}^{-3}$  for L4\_SM root-zone soil moisture.

610

#### 611 4) SOIL MOISTURE SUMMARY METRICS

612 We now discuss the average soil moisture metrics across all reference pixels (section 3b), shown  
613 separately for the 9-km and 36-km reference pixels in Figure 5 (with numerical values listed in  
614 the bottom two rows of Table 4). The most important result is that the average ubRMSE values  
615 for L4\_SM surface soil moisture ( $0.038 \text{ m}^3 \text{ m}^{-3}$ ) and root-zone soil moisture ( $0.030 \text{ m}^3 \text{ m}^{-3}$ ) at the  
616 9-km scale meet the accuracy requirement of  $0.04 \text{ m}^3 \text{ m}^{-3}$ .

617

618 For a more in-depth analysis, we first compare the skill of the L4\_SM and NRv4 estimates. For  
619 the ubRMSE and R metrics and at the 9-km and the 36-km scales, the surface soil moisture skill  
620 of L4\_SM exceeds that of NRv4 by a statistically significant margin (as indicated by the non-

621 overlapping confidence intervals; Figure 5). For example, the 9-km ubRMSE for L4\_SM  
622 surface soil moisture is  $0.038 \text{ m}^3 \text{ m}^{-3}$ , compared to  $0.042 \text{ m}^3 \text{ m}^{-3}$  for NRv4. The corresponding R  
623 values are 0.67 for L4\_SM and 0.58 for NRv4. The average bias is slightly (but not  
624 significantly) worse for L4\_SM ( $0.046 \text{ m}^3 \text{ m}^{-3}$ ) than NRv4 ( $0.043 \text{ m}^3 \text{ m}^{-3}$ ). The results are  
625 similar for root-zone soil moisture, except here the differences between the L4\_SM and NRv4  
626 estimates are not significant (Figure 5). The 9-km ubRMSE for L4\_SM root-zone soil moisture  
627 ( $0.030 \text{ m}^3 \text{ m}^{-3}$ ) is slightly lower than that of NRv4 ( $0.032 \text{ m}^3 \text{ m}^{-3}$ ), and the R value for L4\_SM  
628 (0.70) is higher than that of NRv4 (0.56). The average root-zone soil moisture bias is  
629 remarkably small and slightly better for L4\_SM ( $0.009 \text{ m}^3 \text{ m}^{-3}$ ) than NRv4 ( $0.019 \text{ m}^3 \text{ m}^{-3}$ ).

630

631 A closer look at the metrics for the individual reference pixels (Table 4) reveals that the  
632 ubRMSE and R metrics are worse for L4\_SM than NRv4 at some sites, including Carman and  
633 HOBE. There could be several reasons why the L4\_SM analysis degrades the model-only skill,  
634 including site-specific errors in the radiative transfer modeling. For example, the L4\_SM system  
635 does not account for the heavy dewfall and the variety of different crops at Carman. At HOBE,  
636 the SMOS-based brightness temperature climatology used for rescaling might be impacted by  
637 radio-frequency interference or by the effect of the land-sea contrast in the interferometric  
638 processing (Al Bitar et al. 2012). Nevertheless, the L4\_SM product has, on balance, higher skill  
639 than NRv4. The L4\_SM root-zone ubRMSE is below the  $0.04 \text{ m}^3 \text{ m}^{-3}$  threshold at all 16 (9-km  
640 and 36-km) reference pixels, while the NRv4 ubRMSE exceeds  $0.04 \text{ m}^3 \text{ m}^{-3}$  at 2 of the 3 South  
641 Fork reference pixels. Surface soil moisture estimates from NRv4 fail to meet the  $0.04 \text{ m}^3 \text{ m}^{-3}$   
642 threshold at 18 of the 43 reference pixels. By contrast, L4\_SM surface soil moisture estimates  
643 fail to meet the threshold at only 10 of the 43 reference pixels, including 9-km pixels at Yanco,

644 Carman, St. Josephs, South Fork, Benin, and TxSON. This result further illustrates the key role  
645 played by the assimilation of SMAP observations in meeting the L4\_SM accuracy requirement  
646 (which applies to the average ubRMSE across all 9-km reference pixels; section 3a).

647  
648 Next, we compare the skill values at 9-km reference pixels to those at the 36-km scale.  
649 Generally, the L4\_SM and NRv4 skill at 36 km is better for all three metrics than that at 9 km  
650 (Figure 5), which is consistent with the fact that the model forcing data and the assimilated  
651 SMAP brightness temperature observations are all at resolutions of about 30 km or greater. The  
652 information used to downscale the assimilated information stems only from the land model  
653 parameters, which are at the finer, 9-km resolution. It is therefore not surprising that the L4\_SM  
654 (and NRv4) estimates are more skillful (that is, contain less random error) when averaged to the  
655 36-km scale than at the 9-km scale. Perhaps the biggest difference between the 36-km and 9-km  
656 reference pixel skill is for the surface soil moisture bias (Figure 5b). The smaller bias at the  
657 36-km scale is likely also related to the fact that the grid-cell scale *in situ* measurements for  
658 36-km reference pixels are typically based on more individual sensor locations than those for  
659 9-km reference pixels, resulting in more robust *in situ* estimates of the true long-term mean  
660 conditions at the 36-km scale.

661  
662 Finally, we compare the skill of the surface soil moisture estimates to that of the root-zone  
663 estimates. Across all scales and metrics and for the L4\_SM and NRv4 estimates, the skill of the  
664 root-zone soil moisture estimates is always better than that of the surface estimates (Figure 5).  
665 This result makes sense because there is much more variability in surface soil moisture.

666

667

668 5) SOIL TEMPERATURE SUMMARY METRICS

669 Since the focus of the L4\_SM product is on soil moisture, there is no pre-defined accuracy target  
670 for the L4\_SM surface soil temperature estimates. It is nevertheless instructive to assess their  
671 skill (Figure 6; Table 5), especially given the importance of soil temperature for biophysical  
672 processes and the use of L4\_SM soil temperature estimates as inputs to the SMAP Level-4  
673 Carbon product (Jones et al. 2017). The average surface soil temperature metrics for L4\_SM and  
674 NRv4 are fairly similar across all categories, with average ubRMSE values ranging from 1.6 to  
675 1.8 K (Figure 6a) and average R values of  $\sim 0.97$  (Figure 6c) for 9-km and 36-km estimates at  
676 6am and 6pm. At 6am, surface soil temperature estimates from L4\_SM have a slightly lower  
677 ubRMSE than NRv4 (by  $\sim 0.1$  K) and a slightly higher R value than NRv4 (by  $\sim 0.005$ ), but the  
678 differences are not significant. At 6pm, the L4\_SM and NRv4 ubRMSE and R values are  
679 essentially identical.

680

681 Somewhat bigger differences between the various estimates occur for the average bias in surface  
682 soil temperature (Figure 6b). At 6am, both L4\_SM and NRv4 are biased cold, with NRv4  
683 having a larger (negative) bias of around -2.5 K compared to about -1.8 K for L4\_SM (at both  
684 the 9-km and 36-km scales). This 6am cold bias is consistent with a known nighttime cold bias  
685 in the GEOS-5 modeling system (Chan et al. 2016b). At 6pm, the average bias at the 9-km scale  
686 nearly vanishes for NRv4 (0.1 K), whereas L4\_SM still exhibits a distinct cold bias (-1.1 K).  
687 Note that some of the bias at individual sites might also be caused by instrumentation details  
688 such as the vertical or horizontal installation of the sensors, which impacts the exact depths  
689 where the sensors' thermistors are located.

690

691 The 36-km average bias shown in Figure 6b includes the extreme values at the Ngari reference  
692 pixel in western Tibet, where the 6pm bias in surface soil temperature is -9.1 K for NRv4 and  
693 -12.5 K for L4\_SM (Table 5). The L4\_SM bias at Ngari is not unique for a global modeling  
694 system. In their Table 3, Su et al. (2013) report a diurnal mean bias of -6.9 K at Naqu (in central  
695 Tibet) for surface soil temperature estimates from the operational system of the European Centre  
696 for Medium-Range Weather Forecasts. The reasons for the extreme bias in Tibet are complex.  
697 Most importantly, there is a bias in the GEOS-5 radiation and air temperature forcing data used  
698 in the L4\_SM system compared to the observation-based data of Chen et al. (2011) (not shown).  
699 This forcing bias is likely compounded by errors in the L4\_SM soil texture inputs, soil thermal  
700 parameters, and surface turbulence parameterization (Van der Velde et al. 2009; Zeng et al.  
701 2012; Zheng et al. 2015). If Ngari is excluded from the 36-km reference pixel average, the 6pm  
702 bias values change from -0.5 K to 0.2 K for NRv4 and from -1.7 K to -0.9 K for L4\_SM. More  
703 generally, the increase in the (absolute) bias in the L4\_SM estimates compared to NRv4 is likely  
704 the result of using imperfect brightness temperature rescaling parameters (section 2d), but this  
705 requires further investigation and is left for future study.

706

707 The relatively minor differences between the L4\_SM and NRv4 soil temperature metrics (Figure  
708 6) are not surprising. The L4\_SM brightness temperature analysis has been calibrated primarily  
709 for updating the model forecast soil moisture estimates; soil temperature increments are  
710 relatively small by design (De Lannoy and Reichle 2016a). This strategy mirrors the approach  
711 taken by the SMAP and SMOS (passive) soil moisture retrieval algorithms, which rely on  
712 ancillary soil temperature information that is assumed to be sufficiently accurate to invert  
713 brightness temperature observations into soil moisture estimates.



714

715 *b. Sparse network validation*

716 Figure 7 illustrates the ubRMSE values for the L4\_SM estimates at the sparse network sites. The  
717 gray background shading in the figure also indicates whether a site is within the mask of the  
718 formal accuracy requirement (section 3a). The resulting delineation (Figure 7) suggests, for  
719 example, that sites in the more topographically complex western United States mountain areas  
720 and in the more densely vegetated portions of the eastern United States fall, as expected, outside  
721 the mask. Overall, ubRMSE values range from  $0.02 \text{ m}^3 \text{ m}^{-3}$  to  $0.07 \text{ m}^3 \text{ m}^{-3}$ , with generally lower  
722 error values for root-zone soil moisture than for surface soil moisture (Figure 7). Errors are  
723 generally lowest in dry and mountainous areas in the western United States, where the soil  
724 moisture variability is typically low, thus naturally limiting the ubRMSE values. The ubRMSE  
725 values at the Australian sites are relatively high both inside and outside the mask (on average,  
726  $0.063 \text{ m}^3 \text{ m}^{-3}$  for surface and  $0.056 \text{ m}^3 \text{ m}^{-3}$  for root-zone soil moisture), owing primarily to the  
727 large variability in soil moisture in this region. The R values for the sparse network sites, shown  
728 in Figure 8, range from 0.3 to 0.9, with generally similar correlations for surface and root-zone  
729 soil moisture. There is no obvious spatial pattern across the US networks or the Australian sites,  
730 although the latter exhibit generally high R values.

731

732 Figure 9 shows the average L4\_SM metrics vs. sparse network measurements, broken down by  
733 the exclusion mask of the accuracy requirement (as indicated by the gray shading in Figures 7  
734 and 8). The figure confirms that the L4\_SM ubRMSE values are lower at the sites outside the  
735 mask, with values of  $0.049 \text{ m}^3 \text{ m}^{-3}$  for surface soil moisture and  $0.040 \text{ m}^3 \text{ m}^{-3}$  for root-zone soil  
736 moisture (Figure 9b, Table 6), compared to  $0.054 \text{ m}^3 \text{ m}^{-3}$  and  $0.044 \text{ m}^3 \text{ m}^{-3}$  for surface and root-

737 zone soil moisture, respectively, at sites within the mask (Figure 9a). Again, this result is related  
738 to the much lower variability of soil moisture in the arid regions of the western United States,  
739 which also happen to lie largely in mountainous terrain. The result is reversed for the average  
740 bias. Inside the mask, average bias values are  $0.028 \text{ m}^3 \text{ m}^{-3}$  for surface soil moisture and  $-0.003$   
741  $\text{m}^3 \text{ m}^{-3}$  for root-zone soil moisture (Figure 9c), compared to  $0.078 \text{ m}^3 \text{ m}^{-3}$  for surface soil  
742 moisture and  $0.042 \text{ m}^3 \text{ m}^{-3}$  for root-zone soil moisture, respectively, outside the mask (Figure  
743 9d). This relative performance is at least partly due to the increased topographical complexity  
744 near many of the sites outside of the mask, which are generally even less representative of the  
745 grid-cell average conditions than are sparse network sites within the mask. The values for the  
746 time series correlation coefficients generally range between 0.6 and 0.7 and are more similar  
747 inside and outside the mask (Figure 9e,f). This is expected because the R values are, by  
748 construction, insensitive to bias and to errors in variability.

749

750 Figure 9 also shows the skill of the NRv4 estimates. The surface soil moisture skill in terms of R  
751 is significantly higher (at the 5% level) for L4\_SM than for NRv4, reflecting the additional  
752 information contributed by the assimilation of the SMAP brightness temperature observations in  
753 the L4\_SM system both inside and outside of the exclusion mask. For root-zone soil moisture,  
754 the skill values are very similar for L4\_SM and NRv4. As for the core validation sites, the  
755 typically small differences between L4\_SM and NRv4 estimates reflect the fact that the sparse  
756 network measurements are located in areas where the surface meteorological forcing takes  
757 advantage of high-quality, gauge-based precipitation measurements. Larger improvements from  
758 the assimilation of SMAP observations can be expected in areas where the precipitation forcing

759 inputs are not as well informed by gauge measurements, as demonstrated by Bolten and Crow  
760 (2012) for the assimilation of AMSR-E soil moisture retrievals.

761

762 Table 6 further provides average skill metrics broken down by the IGBP land cover classes  
763 (section 3c). The ubRMSE and R skill of the L4\_SM surface and root-zone soil moisture  
764 estimates is better than that of NRv4 for all IGBP classes except for root-zone soil moisture in  
765 grasslands and urban areas, where NRv4 is better than L4\_SM (but not significantly). The bias  
766 values listed in Table 6 suggest that the mean soil moisture from the L4\_SM estimates is biased  
767 high (that is, wet) for all land cover classes, with similar mean bias values for NRv4. This is  
768 particularly true for the forest class, because *in situ* measurement sites are typically on grassy  
769 areas, regardless of the surrounding land cover. For the forest class, Table 6 shows that the  
770 L4\_SM and NRv4 estimates have the highest bias values,  $\sim 0.1 \text{ m}^3 \text{ m}^{-3}$  for surface soil moisture  
771 and  $0.055 \text{ m}^3 \text{ m}^{-3}$  for root-zone soil moisture (not considering the higher average root-zone bias  
772 at the three sites in the urban class).

773

774

775

776

777

778

## 779 **5. Summary and Conclusions**

780 This study provides a brief overview of the SMAP L4\_SM algorithm and focuses on the  
781 validation of the L4\_SM product using *in situ* soil moisture and temperature measurements from  
782 core validation sites and sparse networks. Based on the core validation site results, the L4\_SM  
783 estimates of surface and root-zone soil moisture meet the accuracy requirement ( $\text{ubRMSE} \leq 0.04$   
784  $\text{m}^3 \text{m}^{-3}$ ). For surface soil moisture, the ubRMSE is  $0.038 \text{ m}^3 \text{m}^{-3}$  at the 9-km scale and  $0.035 \text{ m}^3$   
785  $\text{m}^{-3}$  at the 36-km scale. For root-zone soil moisture, the ubRMSE is  $0.030 \text{ m}^3 \text{m}^{-3}$  at the 9-km  
786 scale and  $0.026 \text{ m}^3 \text{m}^{-3}$  at the 36-km scale (Figure 5). Through the assimilation of SMAP  
787 brightness temperatures, the L4\_SM surface soil moisture estimates are improved significantly  
788 (at the 5% level) compared to model-only NRv4 estimates. The latter have an ubRMSE of  $0.042$   
789  $\text{m}^3 \text{m}^{-3}$  at the 9-km scale and do not meet the L4\_SM accuracy requirement. L4\_SM root-zone  
790 soil moisture estimates are also better (but not significantly) than those of NRv4, which have an  
791 ubRMSE of  $0.032 \text{ m}^3 \text{m}^{-3}$  at the 9-km scale. Similar qualitative results are obtained for the R  
792 metric.

793

794 Surface soil temperature ubRMSE values vs. core validation site measurements range between  
795 1.6 and 1.8 K for 6am and 6pm estimates from L4\_SM and NRv4 at the 9-km and 36-km scales  
796 (Figure 6). The L4\_SM estimates show only minor improvements (not significant) of  $\sim 0.1$  K for  
797 6am (compared to NRv4), with nearly identical 6pm skill values for L4\_SM and NRv4. R  
798 values for surface soil temperature estimates are  $\sim 0.97$ , suggesting that the modeled soil  
799 temperatures adequately capture synoptic and seasonal variations. The L4\_SM product is biased  
800 cold by about  $-2$  K at 6am, which is consistent with a known cold bias in current GEOS-5  
801 products. In the arid, high-elevation environment at Ngari in western Tibet, however, errors in

802 the L4\_SM forcing data and modeling system result in a much larger cold bias of -12.5 K for  
803 surface soil temperature at 6pm.

804

805 The sparse network results corroborate the core validation site findings for a greater variety of  
806 climate and land cover conditions (Figure 9). It is important to keep in mind that the sparse  
807 network skill metrics presented here underestimate the true skill because these metrics are based  
808 on a direct comparison of the L4\_SM product against *in situ* measurements which are subject to  
809 upscaling and other errors. The same is true, to a lesser extent, for the metrics vs. core validation  
810 site measurements, and Chen et al. (2017) quantified the impact of such errors on the R skill of  
811 soil moisture retrievals. Therefore, the sparse network ubRMSE values suggest that the L4\_SM  
812 estimates would meet the formal accuracy requirement across a very wide variety of surface  
813 conditions, beyond those that are covered by the few core validation sites that have been  
814 available to date for formal verification of the accuracy requirement. The sparse network results  
815 thus provide additional confidence in the conclusions drawn from the core validation site  
816 comparisons.

817

818 The core validation site and sparse network results both suggest that the L4\_SM surface soil  
819 moisture is still biased wet (by 0.02-0.05 m<sup>3</sup> m<sup>-3</sup>, on average), while the root-zone soil moisture  
820 bias is smaller (less than 0.01 m<sup>3</sup> m<sup>-3</sup> for the core sites, and 0.016 m<sup>3</sup> m<sup>-3</sup> for the sparse network  
821 sites). The wet bias in surface soil moisture is consistent with the findings of De Lannoy et al.  
822 (2014b), who introduced the revised soil texture and soil hydraulic parameters used here to  
823 address the even stronger bias in earlier versions of the GEOS-5 modeling system (such as those  
824 used in the MERRA-Land and MERRA-2 reanalysis products). The development of the L4\_SM

825 product played an important role in mitigating the bias of GEOS-5 soil moisture estimates, and  
826 work is ongoing to further reduce the remaining bias.

827

828 The skill of the model-only NRv4 estimates (section 2c) rests, to a large degree, on the accuracy  
829 of the precipitation forcing, which relies on the daily, 0.5°, gauge-based CPCU product (except  
830 in Africa and the high latitudes). For the most part, the soil moisture validation against *in situ*  
831 measurements is limited to regions that also have relatively accurate precipitation inputs, which  
832 implies that the model-only (NRv4) skill is already relatively high, thereby limiting the potential  
833 improvements that can be obtained from the assimilation of SMAP observations. In regions with  
834 poor precipitation data, the impact of the SMAP observations should be larger, but the precise  
835 benefit remains unknown in those regions because they also lack soil moisture *in situ*  
836 measurements suitable for validation. In future work, we plan to quantify the skill improvement  
837 against model-only estimates that do not benefit from the use of gauge-based precipitation data.

838

839 The NRv4 and L4\_SM estimates differ in that the NRv4 estimates are from a single-member  
840 model run without perturbations, whereas the L4\_SM estimates are based on an ensemble of  
841 model realizations that experiences perturbations to its model forcing and prognostic variables.  
842 An undesirable, yet at this time unavoidable, side effect of the perturbations regime is that it  
843 leads to biases between the ensemble mean estimates and the estimates from the unperturbed  
844 NRv4 model integration. This is particularly acute in very arid regions, where the perturbations  
845 in soil moisture are, by construction, biased wet because the unperturbed, single-member model  
846 run often remains at the lowest possible soil moisture value, thereby making negative (that is,  
847 drying) perturbations unphysical. Some of the differences between the NRv4 and L4\_SM

848 estimates will therefore partly reflect the impact of the perturbations regime rather than the use  
849 of SMAP observations. We plan to investigate this issue further by generating a model-only  
850 ensemble run with the same perturbations regime as the L4\_SM product but without SMAP  
851 assimilation. Preliminary results based on a small domain suggest that the relative performance  
852 of the L4\_SM estimates and the revised model-only estimates is quite similar to that of L4\_SM  
853 and NRv4.

854

855 Our assessment of the Version 2 L4\_SM data is still quite limited by the period of record. The  
856 two years of data that were available for this study do not yet cover a representative range of  
857 inter-annual variability. As the SMAP observatory and *in situ* networks continue to provide  
858 additional measurements, the reliability of future assessments will increase. Moreover,  
859 enhancements in the GEOS-5 modeling system and in the L-band brightness temperature  
860 climatology needed for bias correction are expected to improve the quality of the L4\_SM  
861 product. In particular, the L-band brightness temperature climatology will eventually be based  
862 on SMAP (as opposed to SMOS) observations. This will improve the brightness temperature  
863 bias correction and permit the use of SMAP data in regions where SMOS observations are  
864 contaminated by radio-frequency interference.

865

866 Finally, the validation of the L4\_SM product against *in situ* measurements must be viewed in  
867 conjunction with other assessments. For example, Crow et al. (2017) demonstrated for the  
868 south-central US that L4\_SM soil moisture estimates have significantly improved utility for  
869 forecasting the streamflow response to future rainfall events (relative to that of soil moisture  
870 retrievals from L-band and higher-frequency Tb observations). Moreover, Reichle et al. (2016a,

871 2017c) evaluate the statistics of the observation-minus-forecast (O-F) residuals and the analysis  
872 increments from the L4\_SM algorithm, which are available wherever and whenever SMAP  
873 observations are assimilated, thereby providing a more global perspective of the algorithm's  
874 performance.

875

876

877



878 **Acknowledgments**

879 Funding for this work was provided by the NASA SMAP mission. Computational resources  
880 were provided by the NASA High-End Computing program through the NASA Center for  
881 Climate Simulation. We are grateful for the datasets and data archiving centers that supported  
882 this work and appreciate those who make the generation, dissemination, and validation of the  
883 L4\_SM product possible, including SMAP team members at JPL, GSFC, and NSIDC and staff at  
884 NOAA CPC, NOAA NCEI, USDA ARS, USDA NRCS, the Oklahoma Climatological Survey,  
885 and Monash University. Erica Tetlock is acknowledged for her help with the Kenaston network,  
886 for which funding was provided by the Canadian Space Agency and by Environment and  
887 Climate Change Canada. We thank three anonymous reviewers for their helpful comments.

888

889 **References**

- 890 Adler, R. F., and Coauthors, 2003: The version 2 Global Precipitation Climatology Project  
891 (GPCP) monthly precipitation analysis (1979–present). *J. Hydrometeor.*, **4**, 1147–1167,  
892 doi:10.1175/1525-7541(2003)004<1147:TVGPCP>2.0.CO;2.
- 893 Al Bitar, A., and Coauthors, 2012: Evaluation of SMOS Soil Moisture Products Over  
894 Continental U.S. Using the SCAN/SNOTEL Network. *IEEE Transactions on Geoscience  
895 and Remote Sensing*, **50**, 1572-1586, doi:10.1109/TGRS.2012.2186581.
- 896 Albergel, C., and Coauthors, 2012: Evaluation of remotely sensed and modelled soil moisture  
897 products using global ground-based *in situ* observations. *Remote Sensing of Environment*,  
898 **118**, 215-226, doi:10.1016/j.rse.2011.11.017.
- 899 Balsamo, G., and Coauthors, 2015: ERA-Interim/Land: A global land surface reanalysis data set,  
900 *Hydrol. Earth Syst. Sci.*, **19**, 389-407, doi:10.5194/hess-19-389-2015.
- 901 Bell, J., and Coauthors, 2013: U.S. Climate Reference Network soil moisture and temperature  
902 observations. *J. Hydrometeor.*, **14**, 977–988, doi:10.1175/JHM-D-12-0146.1.
- 903 Bolten, J.D. and W. T. Crow, 2012: Improved prediction of quasi-global vegetation conditions  
904 using remotely-sensed surface soil moisture. *Geophysical Research Letters*, **39**, L19406,  
905 doi:10.1029/2012GL053470.
- 906 Brodzik, M. J., B. Billingsley, T. Haran, B. Raup, and M. H. Savoie, 2012: EASE-Grid 2.0:  
907 Incremental but Significant Improvements for Earth-Gridded Data Sets. *ISPRS International  
908 Journal of Geo-Information*, **1**, 32-45, doi:10.3390/ijgi1010032.
- 909 Chan, S., E. G. Njoku, and A. Colliander, 2016a: SMAP L1C Radiometer Half-Orbit 36 km  
910 EASE-Grid Brightness Temperatures, Version 3. Boulder, Colorado USA. NASA National

911 Snow and Ice Data Center Distributed Active Archive Center.  
912 doi:10.5067/E51BSP6V3KP7. Last accessed 10 December 2016.

913 Chan, S. K., and Coauthors, 2016b: Assessment of the SMAP Passive Soil Moisture Product.  
914 *IEEE Transactions on Geoscience and Remote Sensing*, **54**, 4994-5007,  
915 doi:10.1109/TGRS.2016.2561938.

916 Chen, F., and Coauthors, 2017: Application of Triple Collocation in Ground-based Validation of  
917 Soil Moisture Active/Passive (SMAP) Level 2 Data Products. *IEEE Journal of Selected*  
918 *Topics in Applied Earth Observations and Remote Sensing*, **10**, 489-502,  
919 doi:10.1109/JSTARS.2016.2569998.

920 Chen, M., W. Shi, P. Xie, V. B. S. Silva, V. E. Kousky, R. W. Higgins, and J. E. Janowiak, 2008:  
921 Assessing objective techniques for gauge-based analyses of global daily precipitation. *J.*  
922 *Geophys. Res.*, **113**, D04110, doi:10.1029/2007JD009132.

923 Chen, Y., K. Yang, J. He, J. Qin, J. Shi, J. Du, and Q. He, 2011: Improving land surface  
924 temperature modeling for dry land of China. *J. Geophys. Res.*, **116**, D20104,  
925 doi:10.1029/2011JD015921.

926 Colliander, A., and Coauthors, 2017: Validation of SMAP surface soil moisture products with  
927 core validation sites. *Remote Sensing of Environment*, **191**, 215-231,  
928 doi:10.1016/j.rse.2017.01.021.

929 Cosh, M. H., T. J. Jackson, P. J. Starks, and G. Heathman, 2006: Temporal stability of surface  
930 soil moisture in the LittleWashita RiverWatershed and its applications in satellite soil  
931 moisture product validation. *J. Hydrol.*, **323**, 168–177, doi:10.1016/j.jhydrol.2005.08.020.

932 Crow, W. T., F. Chen, R. H. Reichle, and Q. Liu, 2017: L band microwave remote sensing and  
933 land data assimilation improve the representation of prestorm soil moisture conditions for

934 hydrologic forecasting. *Geophys. Res. Lett.*, **44**, doi:10.1002/2017GL073642.

935 De Lannoy, G. J. M, R. H. Reichle, and V. R. N. Pauwels, 2013: Global Calibration of the  
936 GEOS-5 L-band Microwave Radiative Transfer Model over Nonfrozen Land Using SMOS  
937 Observations. *Journal of Hydrometeorology*, **14**, 765-785, doi:10.1175/JHM-D-12-092.1.

938 De Lannoy, G. J. M., R. H. Reichle, and J. A. Vrugt, 2014a: Uncertainty Quantification of  
939 GEOS-5 L-Band Radiative Transfer Model Parameters using Bayesian Inference and SMOS  
940 Observations. *Remote Sensing of Environment*, **148**, 146-157, doi:10.1016/j.rse.2014.03.030.

941 De Lannoy, G. J. M., R. D. Koster, R. H. Reichle, S. P. P. Mahanama, and Q. Liu, 2014b: An  
942 Updated Treatment of Soil Texture and Associated Hydraulic Properties in a Global Land  
943 Modeling System. *Journal of Advances in Modeling Earth Systems*, **6**, 957-979,  
944 doi:10.1002/2014MS000330.

945 De Lannoy, G. J. M., R. H. Reichle, J. Peng, Y. Kerr, R. Castro, E. Kim, and Q. Liu, 2015:  
946 Converting between SMOS and SMAP level-1 brightness temperature observations over  
947 nonfrozen land. *IEEE Geosci. Remote Sens. Lett.*, **12**, 1908–1912,  
948 doi:10.1109/LGRS.2015.2437612.

949 De Lannoy, G. J. M., and R. H. Reichle, 2016a: Global Assimilation of Multiangle and  
950 Multipolarization SMOS Brightness Temperature Observations into the GEOS-5 Catchment  
951 Land Surface Model for Soil Moisture Estimation. *Journal of Hydrometeorology*, **17**, 669-  
952 691, doi:10.1175/JHM-D-15-0037.1.

953 De Lannoy, G. J. M., and R. H. Reichle, 2016b: Assimilation of SMOS Brightness Temperatures  
954 or Soil Moisture Retrievals into a Land Surface Model. *Hydrology and Earth System  
955 Sciences*, **20**, 4895-4911, doi:10.5194/hess-20-4895-2016.

956 de Rosnay P., M. Drusch, D. Vasiljevic, G. Balsamo, C. Albergel and L. Isaksen, 2013: A

957 simplified Extended Kalman Filter for the global operational soil moisture analysis at  
958 ECMWF. *Q. J. R. Meteorol. Soc.*, **139**, 1199-1213, doi:10.1002/qj.2023.

959 Dee, D., and Coauthors, 2011: The ERA-Interim reanalysis: Configuration and performance of  
960 the data assimilation system. *Quart. J. Roy. Meteor. Soc.*, **137**, 553–597, doi:10.1002/qj.828.

961 Diamond, H., and Coauthors, 2013: U.S. Climate Reference Network after one decade of  
962 operations: Status and assessment. *Bull. Amer. Meteor. Soc.*, **94**, 485–498,  
963 doi:10.1175/BAMS-D-12-00170.1.

964 Ducharne, A., R. D. Koster, M. J. Suarez, M. Stieglitz, and P. Kumar, 2000: A catchment-based  
965 approach to modeling land surface processes in a general circulation model: 2. Parameter  
966 estimation and model demonstration. *J. Geophys. Res.*, **105**(D20), 24,823-24,838,  
967 doi:10.1029/2000JD900328.

968 Entekhabi, D., and Coauthors, 2010a: The Soil Moisture Active and Passive (SMAP) Mission.  
969 *Proceedings of the IEEE*, **98**, 704-716, doi:10.1109/JPROC.2010.2043918.

970 Entekhabi, D., R. H. Reichle, R. D. Koster, and W. T. Crow, 2010b: Performance Metrics for  
971 Soil Moisture Retrievals and Application Requirements. *Journal of Hydrometeorology*, **11**,  
972 832-840, doi:10.1175/2010JHM1223.1.

973 Entekhabi, D., and Coauthors, 2014: SMAP Handbook, JPL Publication, JPL 400-1567, NASA  
974 Jet Propulsion Laboratory, Pasadena, California, USA, 182 pp. Available online at  
975 <https://smap.jpl.nasa.gov/mission/description>.

976 Gelaro, R., and Coauthors, 2017: MERRA-2 Overview. *J. Climate*, **30**, 5419-5454,  
977 doi:10.1175/JCLI-D-16-0758.1.

978 Huffman, G. J., R. F. Adler, D. T. Bolvin, and G. Gu, 2009: Improving the global precipitation  
979 record: GPCP version 2.1. *Geophys. Res. Lett.*, **36**, L17808, doi:10.1029/2009GL040000.

980 Jackson, R. B., J. Canadell, J. R. Ehleringer, H. A. Mooney, O. E. Sala, and E. D. Schulze, 1996:  
981 A global analysis of root distributions for terrestrial biomes. *Oecologia*, **108**, 389-411,  
982 doi:10.1007/BF00333714.

983 Jackson, T., D. Chen, M. Cosh, F. Li, M. Anderson, C. Walthall, P. Doraiswamy, and E. R.  
984 Hunt, 2004: Vegetation water content mapping using Landsat data derived normalized  
985 difference water index (NDWI) for corn and soybean. *Remote Sensing of Environment*, **92**,  
986 475-482.

987 Jones, L. A., and Coauthors, 2017: The SMAP Level 4 Carbon Product for Monitoring  
988 Ecosystem Land-Atmosphere CO<sub>2</sub> Exchange. *IEEE Transactions on Geosciences and*  
989 *Remote Sensing*, accepted for publication.

990 Kerr, Y. H., and Coauthors, 2010: The SMOS mission: New tool for monitoring key elements of  
991 the global water cycle. *Proc. IEEE*, **98**, 666–687, doi:10.1109/JPROC.2010.2043032.

992 Kerr, Y. H., and Coauthors, 2016: Overview of SMOS performance in terms of global soil  
993 moisture monitoring after six years in operation. *Remote Sensing of Environment*, **180**, 40-63,  
994 doi:10.1016/j.rse.2016.02.042.

995 Koster, R. D., M. J. Suarez, A. Ducharne, M. Stieglitz, and P. Kumar, 2000: A catchment-based  
996 approach to modeling land surface processes in a general circulation model: 1. Model  
997 structure. *J. Geophys. Res.*, **105** (D20), 24,809-24,822, doi:10.1029/2000JD900327.

998 Liu, Q., R. H. Reichle, R. Bindlish, M. H. Cosh, W. T. Crow, R. de Jeu, G. J. M. De Lannoy, G.  
999 J. Huffman, and T. J. Jackson, 2011: The contributions of precipitation and soil moisture  
1000 observations to the skill of soil moisture estimates in a land data assimilation system.  
1001 *Journal of Hydrometeorology*, **12**, 750-765, doi:10.1175/JHM-D-10-05000.1.

1002 Louis, J. E, 1979: A Parametric Model of Vertical Eddy Fluxes in the Atmosphere. *Bound. Lay.*  
1003 *Meteorol.*, **17**, 187-202.

1004 Loveland, T. R., B. C., Reed, J. F. Brown, D. O. Ohlen, Z. Zhu, L. Yang, and J. W. Merchant,  
1005 2000: Development of a global land cover characteristics database and IGBP DISCover from  
1006 1 km AVHRR data. *International Journal of Remote Sensing*, 21, 1303-1330, doi:  
1007 10.1080/014311600210191.

1008 Lucchesi, R. 2013a: File Specification for GEOS-5 FP, NASA GMAO Office Note, No. 4  
1009 (Version 1.0), National Aeronautics and Space Administration, Goddard Space Flight  
1010 Center, Greenbelt, Maryland, USA, 63pp. Available online at  
1011 <http://gmao.gsfc.nasa.gov/pubs>.

1012 Lucchesi, R. 2013b: File Specification for GEOS-5 FP-IT, NASA GMAO Office Note, No. 2  
1013 (Version 1.2), National Aeronautics and Space Administration, Goddard Space Flight  
1014 Center, Greenbelt, Maryland, USA, 60pp. Available online at  
1015 <http://gmao.gsfc.nasa.gov/pubs>.

1016 Mahanama, S. P., R. D. Koster, G. K. Walker, L. L. Takacs, R. H. Reichle, G. De Lannoy, Q.  
1017 Liu, B. Zhao, and M. J. Suarez, 2015: Land Boundary Conditions for the Goddard Earth  
1018 Observing System Model Version 5 (GEOS-5) Climate Modeling System - Recent Updates  
1019 and Data File Descriptions. *NASA/TM-2015-104606*, Vol. **39**, National Aeronautics and  
1020 Space Administration, Goddard Space Flight Center, Greenbelt, Maryland, USA, 55 pp.  
1021 Available from <http://gmao.gsfc.nasa.gov/pubs>.

1022 McPherson, R. A., and Coauthors, 2007: Statewide Monitoring of the Mesoscale Environment:  
1023 A Technical Update on the Oklahoma Mesonet. *J. Atmos. Oceanic Technol.*, **24**, 301-321,  
1024 doi: 10.1175/JTECH1976.1.

1025 Mladenova, I.E., and Coauthors, 2014: Remote monitoring of soil moisture using passive  
1026 microwave-based techniques — theoretical basis and overview of selected algorithms for  
1027 AMSR-E. *Remote Sens. Environ.*, **144**, 197-213, doi: 10.1016/j.rse.2014.01.013.

1028 MODIS, 2008: Leaf Area Index - Fraction of Photosynthetically Active Radiation 8-Day L4  
1029 Global 1km (MOD15A2 v005). NASA EOSDIS Land Processes DAAC, USGS Earth  
1030 Resources Observation and Science (EROS) Center, Sioux Falls, South Dakota  
1031 (<https://lpdaac.usgs.gov>), accessed 28 July 2015, at  
1032 <https://e4ftl01.cr.usgs.gov/MOLT/MOD15A2.005>.

1033 Parinussa, R. M., T. R. H. Holmes, N. Wanders, W. A. Dorigo, and R. A. M. de Jeu, 2015: A  
1034 Preliminary Study toward Consistent Soil Moisture from AMSR2. *J. Hydrometeor.*, **16**,  
1035 932–947, doi: 10.1175/JHM-D-13-0200.1.

1036 Patton, J., and B. Hornbuckle, 2013: Initial Validation of SMOS Vegetation Optical Thickness in  
1037 Iowa, *IEEE Geoscience and Remote Sensing Letters*, **10**, 647-651,  
1038 doi:10.1109/LGRS.2012.2216498.

1039 Piepmeier, J. R., and Coauthors, 2017: SMAP L-Band Microwave Radiometer: Instrument  
1040 Design and First Year on Orbit. *IEEE Transactions on Geoscience and Remote Sensing*, **55**,  
1041 1954-1966, doi:10.1109/TGRS.2016.2631978.

1042 Reichle, R. H., and Q. Liu, 2014: Observation-Corrected Precipitation Estimates in GEOS-5.  
1043 *NASA Technical Report Series on Global Modeling and Data Assimilation, NASA/TM-2014-*  
1044 *104606*, Vol. **35**, National Aeronautics and Space Administration, Goddard Space Flight  
1045 Center, Greenbelt, Maryland, USA, 18pp. Available online at  
1046 <http://gmao.gsfc.nasa.gov/pubs>.



1047 Reichle, R. H., R. D. Koster, G. J. M. De Lannoy, B. A. Forman, Q. Liu, S. P. P. Mahanama, and  
1048 A. Touré, 2011: Assessment and enhancement of MERRA land surface hydrology estimates.  
1049 *J. Climate*, **24**, 6322–6338, doi:10.1175/JCLI-D-10-05033.1.

1050 Reichle, R. H., R. Koster, G. De Lannoy, W. Crow, and J. Kimball, 2014: SMAP Level 4  
1051 Surface and Root Zone Soil Moisture Data Product: L4\_SM Algorithm Theoretical Basis  
1052 Document (Revision A). Soil Moisture Active Passive (SMAP) Mission Science Document.  
1053 JPL D-66483, Jet Propulsion Laboratory, Pasadena, CA. Available online at  
1054 [https://nsidc.org/sites/nsidc.org/files/files/data/smap/272\\_L4\\_SM\\_RevA\\_web.pdf](https://nsidc.org/sites/nsidc.org/files/files/data/smap/272_L4_SM_RevA_web.pdf)

1055 Reichle, R. H., R. A. Lucchesi, J. V. Ardizzone, G.-K. Kim, E. B. Smith, and B. H. Weiss,  
1056 2015a: Soil Moisture Active Passive (SMAP) Mission Level 4 Surface and Root Zone Soil  
1057 Moisture (L4\_SM) Product Specification Document, *NASA GMAO Office Note, No. 10*  
1058 (*Version 1.4*), National Aeronautics and Space Administration, Goddard Space Flight  
1059 Center, Greenbelt, Maryland, USA, 82pp. Available online at  
1060 <http://gmao.gsfc.nasa.gov/pubs>.

1061 Reichle, R. H., and Coauthors, 2015b: Soil Moisture Active Passive (SMAP) Project Assessment  
1062 Report for the Beta-Release L4\_SM Data Product. *NASA Technical Report Series on Global*  
1063 *Modeling and Data Assimilation, NASA/TM-2015-104606, Vol. 40*, National Aeronautics  
1064 and Space Administration, Goddard Space Flight Center, Greenbelt, Maryland, USA, 63pp.  
1065 Available online at <http://gmao.gsfc.nasa.gov/pubs>.

1066 Reichle, R. H., and Coauthors, 2016a: Soil Moisture Active Passive Mission L4\_SM Data  
1067 Product Assessment (Version 2 Validated Release), NASA GMAO Office Note, No. 12  
1068 (Version 1.0), National Aeronautics and Space Administration, Goddard Space Flight  
1069 Center, Greenbelt, Maryland, USA, 55pp. Available online at

1070 <http://gmao.gsfc.nasa.gov/pubs>.

1071 Reichle, R. H., G. De Lannoy, R. D. Koster, W. T. Crow, and J. S. Kimball, 2016b: SMAP L4 9  
1072 km EASE-Grid Surface and Root Zone Soil Moisture Analysis Update, Version 2. Boulder,  
1073 Colorado USA. NASA National Snow and Ice Data Center Distributed Active Archive  
1074 Center. doi:10.5067/JJY2V0GJNFRZ. Last accessed 10 December 2016.

1075 Reichle, R. H., G. De Lannoy, R. D. Koster, W. T. Crow, and J. S. Kimball, 2016c: SMAP L4 9  
1076 km EASE-Grid Surface and Root Zone Soil Moisture Land Model Constants, Version 2.  
1077 Boulder, Colorado USA. NASA National Snow and Ice Data Center Distributed Active  
1078 Archive Center. doi:10.5067/VBRUC1AFRQ22. Last accessed 10 December 2016.

1079 Reichle, R. H., G. De Lannoy, R. D. Koster, W. T. Crow, and J. S. Kimball, 2016d: SMAP L4 9  
1080 km EASE-Grid Surface and Root Zone Soil Moisture Geophysical Data, Version 2.  
1081 Boulder, Colorado USA. NASA National Snow and Ice Data Center Distributed Active  
1082 Archive Center. doi:10.5067/YK70EPDHNF0L. Last accessed 10 December 2016.

1083 Reichle, R. H., Q. Liu, R. D. Koster, C. S. Draper, S. P. P. Mahanama, and G. S. Partyka, 2017a:  
1084 Land surface precipitation in MERRA-2, *Journal of Climate*, **30**, 1643-1664,  
1085 doi:10.1175/JCLI-D-16-0570.1.

1086 Reichle, R. H., and Coauthors, 2017b: Assessment of MERRA-2 land surface hydrology  
1087 estimates. *Journal of Climate*, **30**, 2937–2960, doi:10.1175/JCLI-D-16-0720.1.

1088 Reichle, R. H., and Coauthors, 2017c: Global Assessment of the SMAP Level 4 Surface and  
1089 Root-Zone Soil Moisture Product Using Assimilation Diagnostics. *Journal of*  
1090 *Hydrometeorology*, submitted.

1091 Saha, S., and Coauthors, 2010: The NCEP Climate Forecast System Reanalysis. *Bull. Amer.*

1092 *Meteor. Soc.*, **91**, 1015–1057, doi:10.1175/2010BAMS3001.1.

1093 Schaefer, G. L., M. H. Cosh, and T. J. Jackson, 2007: The USDA Natural Resources  
1094 Conservation Service Soil Climate Analysis Network (SCAN). *J. Atmos. Oceanic Technol.*,  
1095 **24**, 2073–2077.

1096 Smith, A., and Coauthors, 2012: The Murrumbidgee soil moisture monitoring network data set.  
1097 *Water Resour. Res.*, **48**, W07701, doi:10.1029/2012WR011976.

1098 Su, Z., P. de Rosnay, J. Wen, L. Wang, and Y. Zeng, 2013: Evaluation of ECMWF's soil  
1099 moisture analyses using observations on the Tibetan Plateau. *J. Geophys. Res. Atmos.*, **118**,  
1100 5304–5318, doi:10.1002/jgrd.50468.

1101 Stieglitz, M., A. Ducharne, R. Koster, and M. Suarez, 2001: The Impact of Detailed Snow  
1102 Physics on the Simulation of Snow Cover and Subsurface Thermodynamics at Continental  
1103 Scales. *J. Hydrometeor.*, **2**, 228–242.

1104 Van der Velde, R., Z. Su, M. Ek, M. Rodell, and Y. Ma, 2009: Influence of thermodynamic soil  
1105 and vegetation parameterizations on the simulation of soil temperature states and surface  
1106 fluxes by the noah LSM over a tibetan plateau site. *Hydrology and Earth System Sciences*,  
1107 **13**, 759.

1108 Wagner, W., and Coauthors, 2013: The ASCAT Soil Moisture Product: A Review of its  
1109 Specifications, Validation Results, and Emerging Applications. *Meteorologische Zeitschrift*,  
1110 **22**, 5–33, doi:10.1127/0941-2948/2013/0399.

1111 Wösten, J., Y. A. Pachepsky, and W. Rawls, 2001: Pedotransfer functions: Bridging the gap  
1112 between available basic soil data and missing soil hydraulic characteristics. *J. Hydrol.*, **251**,  
1113 123–150, doi:10.1016/S0022-1694(01)00464-4.

- 1114 Xie, P., M. Chen, S. Yang, A. Yatagai, T. Hayasaka, Y. Fukushima, and C. Liu, 2007: A gauge-  
1115 based analysis of daily precipitation over East Asia. *J. Hydrometeor.*, **8**, 607–626,  
1116 doi:10.1175/JHM583.1
- 1117 Zeng, X., Z. Wang, and A. Wang, 2012: Surface Skin Temperature and the Interplay between  
1118 Sensible and Ground Heat Fluxes over Arid Regions. *J. Hydrometeor.*, **13**, 1359–1370,  
1119 doi:10.1175/JHM-D-11-0117.1.
- 1120 Zheng, D., and Coauthors, 2015: Augmentations to the Noah Model Physics for Application to  
1121 the Yellow River Source Area. Part II: Turbulent Heat Fluxes and Soil Heat Transport. *J.*  
1122 *Hydrometeor.*, **16**, 2677–2694, doi:10.1175/JHM-D-14-0199.1.

1123  
1124

1125 **Tables**

1126

Site Name	Country	Climate Regime	Land Cover	Reference Pixel										
				ID	Latitude [degree]	Longitude [degree]	Horizontal Scale [km]	Depth of Deepest Sensor [m]	Number of Sensors (Surface Soil Moisture)			Number of Sensors (Root Zone Profiles)		
									Min	Mean	Max	Min	Mean	Max
REMEDHUS	Spain	Temperate	Croplands	<b>03013602</b>	<b>41.28</b>	<b>-5.41</b>	<b>36</b>	<b>0.05</b>	<b>8</b>	<b>14.6</b>	<b>17</b>	n/a	n/a	n/a
				03010903	41.42	-5.37	9	0.05	4	4.0	4	n/a	n/a	n/a
				03010908	41.32	-5.27	9	0.05	4	4.0	4	n/a	n/a	n/a
Reynolds Creek	USA	Arid	Grasslands	<b>04013603</b>	<b>43.14</b>	<b>-116.76</b>	<b>36</b>	<b>0.05</b>	<b>8</b>	<b>9.5</b>	<b>11</b>	n/a	n/a	n/a
				04010907	43.19	-116.72	9	0.05	4	4.0	4	n/a	n/a	n/a
				04010910	43.09	-116.81	9	0.05	4	4.0	4	n/a	n/a	n/a
Yanco	Australia (New South Wales)	Arid	Cropland / natural mosaic	<b>07013601</b>	<b>-34.85</b>	<b>146.17</b>	<b>36</b>	<b>0.75</b>	<b>9</b>	<b>25.4</b>	<b>28</b>	<b>7</b>	<b>7.0</b>	<b>7</b>
				07010902	-34.72	146.13	9	0.05	8	10.2	11	n/a	n/a	n/a
				07010916	-34.98	146.31	9	0.05	8	10.3	11	n/a	n/a	n/a
Carman	Canada (Manitoba)	Cold	Croplands	<b>09013610</b>	<b>49.61</b>	<b>-97.94</b>	<b>36</b>	<b>0.05</b>	<b>8</b>	<b>17.9</b>	<b>20</b>	n/a	n/a	n/a
				09010906	49.67	-97.98	9	0.05	8	10.1	11	n/a	n/a	n/a
Ngari	China (Tibet)	Cold	Barren / sparse	<b>12033601</b>	<b>32.41</b>	<b>79.98</b>	<b>36</b>	<b>0.05</b>	<b>6</b>	<b>6.0</b>	<b>6</b>	n/a	n/a	n/a
Walnut Gulch	USA (Arizona)	Arid	Shrub open	<b>16013603</b>	<b>31.68</b>	<b>-110.04</b>	<b>36</b>	<b>0.05</b>	<b>8</b>	<b>10.6</b>	<b>12</b>	n/a	n/a	n/a
				16010906	31.72	-110.09	9	0.05	8	9.6	11	n/a	n/a	n/a
				16010907	31.72	-109.99	9	0.05	8	10.4	11	n/a	n/a	n/a
				16010913	31.83	-110.90	9	0.05	7	7.0	7	n/a	n/a	n/a
Little Washita	USA (Oklahoma)	Temperate	Grasslands	<b>16023602</b>	<b>34.88</b>	<b>-98.09</b>	<b>36</b>	<b>0.45</b>	<b>8</b>	<b>15.5</b>	<b>18</b>	<b>8</b>	<b>13.4</b>	<b>17</b>
				16020907	34.92	-98.04	9	0.45	4	4.0	4	4	4.0	4
Fort Cobb	USA (Oklahoma)	Temperate	Grasslands	<b>16033602</b>	<b>35.42</b>	<b>-98.62</b>	<b>36</b>	<b>0.45</b>	<b>8</b>	<b>12.3</b>	<b>13</b>	<b>8</b>	<b>11.1</b>	<b>13</b>
				16030911	35.38	-98.57	9	0.45	4	4.0	4	4	4.0	4
				16030916	35.29	-98.48	9	0.45	4	4.0	4	4	4.0	4
Little River	USA (Georgia)	Temperate	Cropland / natural mosaic	<b>16043602</b>	<b>31.60</b>	<b>-83.59</b>	<b>36</b>	<b>0.30</b>	<b>8</b>	<b>19.8</b>	<b>23</b>	<b>8</b>	<b>18.6</b>	<b>22</b>
				16040901	31.72	-83.73	9	0.30	8	8.0	8	6	6.0	6
St Josephs	USA (Indiana)	Temperate	Croplands	16060907	41.45	-84.97	9	0.05	8	8.2	9	n/a	n/a	n/a
South Fork	USA (Iowa)	Cold	Croplands	<b>16073602</b>	<b>42.47</b>	<b>-93.39</b>	<b>36</b>	<b>0.50</b>	<b>8</b>	<b>14.4</b>	<b>15</b>	<b>8</b>	<b>13.1</b>	<b>15</b>
				16070909	42.42	-93.53	9	0.50	4	4.0	4	4	4.0	4
				16070911	42.42	-93.35	9	0.50	4	4.0	4	4	4.0	4
Monte Buey	Argentina	Temperate	Croplands	<b>19023601</b>	<b>-32.96</b>	<b>-62.52</b>	<b>36</b>	<b>0.05</b>	<b>8</b>	<b>10.3</b>	<b>13</b>	n/a	n/a	n/a
				19020902	-33.01	-62.49	9	0.05	5	5.0	5	n/a	n/a	n/a
Tonzi Ranch	USA	Temperate	Savannas woody	<b>25013601</b>	<b>38.47</b>	<b>-121.00</b>	<b>36</b>	<b>0.05</b>	<b>8</b>	<b>17.5</b>	<b>26</b>	n/a	n/a	n/a
				25010911	38.43	-120.95	9	0.05	8	17.5	26	n/a	n/a	n/a
Kenaston	Canada (Saskatchewan)	Cold	Croplands	<b>27013601</b>	<b>51.45</b>	<b>-106.46</b>	<b>36</b>	<b>0.50</b>	<b>8</b>	<b>25.7</b>	<b>28</b>	<b>8</b>	<b>23.1</b>	<b>28</b>
				27010910	51.39	-106.51	9	0.05	8	8.0	8	n/a	n/a	n/a
				27010911	51.39	-106.42	9	0.50	8	13.6	14	8	12.2	14
Valencia	Spain	Cold	Savannas woody	41010906	39.57	-1.26	9	0.05	6	6.0	6	n/a	n/a	n/a
				<b>45013601</b>	<b>13.59</b>	<b>3.65</b>	<b>36</b>	<b>0.05</b>	<b>6</b>	<b>6.0</b>	<b>6</b>	n/a	n/a	n/a
Niger	Niger	Arid	Grassland	45010902	13.55	2.69	9	0.05	4	4.0	4	n/a	n/a	n/a
				<b>45023601</b>	<b>9.77</b>	<b>1.68</b>	<b>36</b>	<b>0.05</b>	<b>7</b>	<b>7.0</b>	<b>7</b>	n/a	n/a	n/a
Benin	Benin	Tropical	Savannas	45020902	9.80	1.73	9	0.05	5	5.0	5	n/a	n/a	n/a
				<b>48013601</b>	<b>30.31</b>	<b>-98.78</b>	<b>36</b>	<b>0.50</b>	<b>10</b>	<b>33.2</b>	<b>35</b>	<b>10</b>	<b>26.3</b>	<b>28</b>
TxSON	USA (Texas)	Temperate	Grasslands	48010902	30.43	-98.82	9	0.50	8	9.9	11	8	8.6	10
				48010911	30.27	-98.73	9	0.50	8	14.4	15	8	13.7	14
				<b>67013601</b>	<b>55.97</b>	<b>9.10</b>	<b>36</b>	<b>0.05</b>	<b>8</b>	<b>15.1</b>	<b>21</b>	n/a	n/a	n/a
HOBE	Denmark	Temperate	Croplands	<b>67013601</b>	<b>55.97</b>	<b>9.10</b>	<b>36</b>	<b>0.05</b>	<b>8</b>	<b>15.1</b>	<b>21</b>	n/a	n/a	n/a

1127

1128 TABLE 1. Core validation sites and reference pixels. Information for 36-km reference pixels is

1129 shown in bold.

1130

	Surface soil moisture		Root zone soil moisture		Surface Soil Temperature (6am)		Surface Soil Temperature (6pm)	
	36 km	9 km	36 km	9 km	36 km	9 km	36 km	9 km
Horizontal scale	36 km	9 km	36 km	9 km	36 km	9 km	36 km	9 km
Number of different core sites	17	17	7	6	14	12	14	13
Number of reference pixels	17	26	7	9	14	21	14	22

1131

1132 TABLE 2. Number of different core sites and number of reference pixels used in the soil moisture  
 1133 and temperature validation.

1134

1135

1136

Network	Area	Sensor Depths (cm)	N	
			Surface Soil Moisture	Root Zone Soil Moisture
SCAN	USA	5, 10, 20	135	129
USCRN	USA	5, 10, 20	111	87
OK Mesonet	Oklahoma	5, 25, 60	118	77
OzNet	Australia	4, 45	42	18
<b>All Networks</b>			<b>406</b>	<b>311</b>

1137

1138 TABLE 3. Overview of sparse networks, with indication of the sensor depths and number of sites

1139 (N) used here.

1140

Site Name	Reference Pixel		Surface Soil Moisture									Root Zone Soil Moisture								
	ID	Horiz. Scale [km]	ubRMSE [ $m^3 m^{-3}$ ]			Bias [ $m^3 m^{-3}$ ]			R [-]			ubRMSE [ $m^3 m^{-3}$ ]			Bias [ $m^3 m^{-3}$ ]			R [-]		
			NRv4	L4_SM Vv2030	95% Conf. Interval	NRv4	L4_SM Vv2030	95% Conf. Interval	NRv4	L4_SM Vv2030	95% Conf. Interval	NRv4	L4_SM Vv2030	95% Conf. Interval	NRv4	L4_SM Vv2030	95% Conf. Interval	NRv4	L4_SM Vv2030	95% Conf. Interval
REMEDHUS	03013602	36	<b>0.027</b>	<b>0.028</b>	<b>±0.005</b>	<b>0.068</b>	<b>0.072</b>	<b>±0.007</b>	<b>0.78</b>	<b>0.77</b>	<b>±0.08</b>	n/a	n/a	n/a	n/a	n/a	n/a	n/a	n/a	n/a
	03010903	9	0.024	<i>0.029</i>	±0.005	0.142	<i>0.150</i>	±0.007	0.52	0.46	±0.14	n/a	n/a	n/a	n/a	n/a	n/a	n/a	n/a	n/a
	03010908	9	0.035	<i>0.038</i>	±0.007	0.013	<i>0.015</i>	±0.009	0.68	0.63	±0.10	n/a	n/a	n/a	n/a	n/a	n/a	n/a	n/a	n/a
Reynolds Creek	04013603	36	<b>0.032</b>	<b>0.027</b>	<b>±0.008</b>	<b>0.025</b>	<b>0.033</b>	<b>±0.011</b>	<b>0.65</b>	<b>0.78</b>	<b>±0.18</b>	n/a	n/a	n/a	n/a	n/a	n/a	n/a	n/a	n/a
	04010907	9	0.032	<i>0.031</i>	±0.010	-0.005	<i>-0.001</i>	±0.013	0.33	0.45	±0.26	n/a	n/a	n/a	n/a	n/a	n/a	n/a	n/a	n/a
	04010910	9	0.036	<i>0.029</i>	±0.018	0.042	<i>0.039</i>	±0.022	0.62	0.76	±0.22	n/a	n/a	n/a	n/a	n/a	n/a	n/a	n/a	n/a
Yanco	07013601	36	<b>0.065</b>	<b>0.038</b>	<b>±0.019</b>	<b>0.005</b>	<b>0.036</b>	<b>±0.025</b>	<b>0.83</b>	<b>0.93</b>	<b>±0.08</b>	<b>0.017</b>	<b>0.020</b>	<b>±0.010</b>	<b>-0.100</b>	<b>-0.079</b>	<b>±0.012</b>	<b>0.89</b>	<b>0.95</b>	<b>±0.17</b>
	07010902	9	0.084	<i>0.057</i>	±0.017	-0.017	<i>0.010</i>	±0.023	0.83	0.91	±0.07	n/a	n/a	n/a	n/a	n/a	n/a	n/a	n/a	n/a
	07010916	9	0.068	<i>0.043</i>	±0.019	0.028	<i>0.068</i>	±0.025	0.77	0.91	±0.10	n/a	n/a	n/a	n/a	n/a	n/a	n/a	n/a	n/a
Carman	09013610	36	<b>0.025</b>	<b>0.038</b>	<b>±0.004</b>	<b>-0.080</b>	<b>-0.066</b>	<b>±0.005</b>	<b>0.60</b>	<b>0.45</b>	<b>±0.10</b>	n/a	n/a	n/a	n/a	n/a	n/a	n/a	n/a	n/a
	09010906	9	0.031	<i>0.050</i>	±0.005	0.043	<i>0.080</i>	±0.007	0.53	0.26	±0.14	n/a	n/a	n/a	n/a	n/a	n/a	n/a	n/a	n/a
Ngari	12033601	36	<b>0.046</b>	<b>0.037</b>	<b>±0.017</b>	<b>0.000</b>	<b>0.011</b>	<b>±0.022</b>	<b>0.78</b>	<b>0.77</b>	<b>±0.22</b>	n/a	n/a	n/a	n/a	n/a	n/a	n/a	n/a	n/a
Walnut Gulch	16013603	36	<b>0.033</b>	<b>0.031</b>	<b>±0.003</b>	<b>0.030</b>	<b>0.039</b>	<b>±0.005</b>	<b>0.58</b>	<b>0.67</b>	<b>±0.09</b>	n/a	n/a	n/a	n/a	n/a	n/a	n/a	n/a	n/a
	16010906	9	0.028	<i>0.030</i>	±0.003	0.019	<i>0.034</i>	±0.005	0.69	0.68	±0.08	n/a	n/a	n/a	n/a	n/a	n/a	n/a	n/a	n/a
	16010907	9	0.026	<i>0.031</i>	±0.003	0.039	<i>0.050</i>	±0.005	0.68	0.66	±0.08	n/a	n/a	n/a	n/a	n/a	n/a	n/a	n/a	n/a
	16010913	9	0.036	<i>0.034</i>	±0.006	0.075	<i>0.081</i>	±0.009	0.60	0.65	±0.15	n/a	n/a	n/a	n/a	n/a	n/a	n/a	n/a	n/a
Little Washita	16023602	36	<b>0.037</b>	<b>0.033</b>	<b>±0.004</b>	<b>-0.004</b>	<b>-0.015</b>	<b>±0.006</b>	<b>0.73</b>	<b>0.81</b>	<b>±0.05</b>	<b>0.029</b>	<b>0.024</b>	<b>±0.005</b>	<b>-0.037</b>	<b>-0.043</b>	<b>±0.007</b>	<b>0.87</b>	<b>0.88</b>	<b>±0.09</b>
	16020907	9	0.037	<i>0.034</i>	±0.006	-0.015	<i>-0.026</i>	±0.009	0.71	0.78	±0.07	0.030	<i>0.030</i>	±0.009	-0.039	<i>-0.043</i>	±0.012	0.82	0.76	±0.16
Fort Cobb	16033602	36	<b>0.038</b>	<b>0.034</b>	<b>±0.004</b>	<b>0.027</b>	<b>0.028</b>	<b>±0.005</b>	<b>0.70</b>	<b>0.78</b>	<b>±0.06</b>	<b>0.024</b>	<b>0.025</b>	<b>±0.004</b>	<b>0.020</b>	<b>0.025</b>	<b>±0.005</b>	<b>0.76</b>	<b>0.79</b>	<b>±0.12</b>
	16030911	9	0.043	<i>0.038</i>	±0.006	0.027	<i>0.033</i>	±0.008	0.71	0.77	±0.07	0.029	<i>0.032</i>	±0.007	0.020	<i>0.031</i>	±0.009	0.69	0.74	±0.18
	16030916	9	0.039	<i>0.038</i>	±0.005	-0.004	<i>-0.008</i>	±0.007	0.60	0.68	±0.07	0.027	<i>0.030</i>	±0.006	-0.029	<i>-0.026</i>	±0.009	0.61	0.62	±0.22
Little River	16043602	36	<b>0.044</b>	<b>0.035</b>	<b>±0.004</b>	<b>0.102</b>	<b>0.093</b>	<b>±0.006</b>	<b>0.68</b>	<b>0.76</b>	<b>±0.09</b>	<b>0.033</b>	<b>0.025</b>	<b>±0.005</b>	<b>0.073</b>	<b>0.063</b>	<b>±0.007</b>	<b>0.81</b>	<b>0.84</b>	<b>±0.11</b>
	16040901	9	0.045	<i>0.038</i>	±0.005	0.128	<i>0.115</i>	±0.007	0.58	0.64	±0.13	0.039	<i>0.032</i>	±0.006	0.125	<i>0.109</i>	±0.008	0.55	0.65	±0.20
St Josephs	16060907	9	0.053	<i>0.050</i>	±0.012	0.111	<i>0.094</i>	±0.017	0.43	0.60	±0.25	n/a	n/a	n/a	n/a	n/a	n/a	n/a	n/a	n/a
South Fork	16073602	36	<b>0.058</b>	<b>0.044</b>	<b>±0.008</b>	<b>0.077</b>	<b>0.045</b>	<b>±0.011</b>	<b>0.23</b>	<b>0.65</b>	<b>±0.11</b>	<b>0.040</b>	<b>0.031</b>	<b>±0.006</b>	<b>0.024</b>	<b>-0.012</b>	<b>±0.009</b>	<b>0.11</b>	<b>0.56</b>	<b>±0.26</b>
	16070909	9	0.064	<i>0.043</i>	±0.008	0.029	<i>-0.009</i>	±0.011	0.11	0.71	±0.12	0.045	<i>0.029</i>	±0.007	-0.035	<i>-0.081</i>	±0.010	0.06	0.70	±0.25
	16070911	9	0.070	<i>0.053</i>	±0.010	0.075	<i>0.039</i>	±0.013	0.08	0.62	±0.12	0.044	<i>0.031</i>	±0.008	0.028	<i>-0.014</i>	±0.010	0.03	0.58	±0.29
Monte Buey	19023601	36	<b>0.044</b>	<b>0.034</b>	<b>±0.010</b>	<b>-0.043</b>	<b>-0.035</b>	<b>±0.014</b>	<b>0.65</b>	<b>0.79</b>	<b>±0.07</b>	n/a	n/a	n/a	n/a	n/a	n/a	n/a	n/a	n/a
	19020902	9	0.037	<i>0.029</i>	±0.009	-0.038	<i>-0.025</i>	±0.012	0.60	0.83	±0.09	n/a	n/a	n/a	n/a	n/a	n/a	n/a	n/a	n/a
Tonzi Ranch	25013601	36	<b>0.042</b>	<b>0.032</b>	<b>±0.010</b>	<b>0.029</b>	<b>0.047</b>	<b>±0.014</b>	<b>0.92</b>	<b>0.95</b>	<b>±0.06</b>	n/a	n/a	n/a	n/a	n/a	n/a	n/a	n/a	n/a
	25010911	9	0.046	<i>0.037</i>	±0.011	0.033	<i>0.044</i>	±0.015	0.90	0.93	±0.07	n/a	n/a	n/a	n/a	n/a	n/a	n/a	n/a	n/a
Kenaston	27013601	36	<b>0.038</b>	<b>0.034</b>	<b>±0.005</b>	<b>0.010</b>	<b>0.012</b>	<b>±0.007</b>	<b>0.51</b>	<b>0.63</b>	<b>±0.09</b>	<b>0.020</b>	<b>0.023</b>	<b>±0.005</b>	<b>-0.043</b>	<b>-0.041</b>	<b>±0.007</b>	<b>0.53</b>	<b>0.63</b>	<b>±0.27</b>
	27010910	9	0.034	<i>0.035</i>	±0.009	0.009	<i>0.016</i>	±0.012	0.61	0.61	±0.12	n/a	n/a	n/a	n/a	n/a	n/a	n/a	n/a	n/a
	27010911	9	0.040	<i>0.040</i>	±0.008	-0.020	<i>-0.021</i>	±0.011	0.56	0.54	±0.11	0.018	<i>0.023</i>	±0.003	-0.069	<i>-0.070</i>	±0.004	0.63	0.63	±0.18
Valencia	41010906	9	0.025	<i>0.023</i>	±0.005	0.104	<i>0.109</i>	±0.007	0.44	0.51	±0.16	n/a	n/a	n/a	n/a	n/a	n/a	n/a	n/a	n/a
Niger	45013601	36	<b>0.030</b>	<b>0.030</b>	<b>±0.005</b>	<b>-0.001</b>	<b>0.022</b>	<b>±0.007</b>	<b>0.40</b>	<b>0.62</b>	<b>±0.20</b>	n/a	n/a	n/a	n/a	n/a	n/a	n/a	n/a	n/a
	45010902	9	0.032	<i>0.033</i>	±0.004	0.006	<i>0.030</i>	±0.006	0.31	0.52	±0.17	n/a	n/a	n/a	n/a	n/a	n/a	n/a	n/a	n/a
Benin	45023601	36	<b>0.050</b>	<b>0.048</b>	<b>±0.016</b>	<b>0.059</b>	<b>0.037</b>	<b>±0.021</b>	<b>0.62</b>	<b>0.66</b>	<b>±0.20</b>	n/a	n/a	n/a	n/a	n/a	n/a	n/a	n/a	n/a
	45020902	9	0.050	<i>0.047</i>	±0.016	0.053	<i>0.036</i>	±0.021	0.68	0.72	±0.17	n/a	n/a	n/a	n/a	n/a	n/a	n/a	n/a	n/a
TxSON	48013601	36	<b>0.041</b>	<b>0.036</b>	<b>±0.008</b>	<b>0.084</b>	<b>0.086</b>	<b>±0.010</b>	<b>0.82</b>	<b>0.87</b>	<b>±0.08</b>	<b>0.036</b>	<b>0.033</b>	<b>±0.016</b>	<b>0.034</b>	<b>0.038</b>	<b>±0.020</b>	<b>0.92</b>	<b>0.86</b>	<b>±0.19</b>
	48010902	9	0.039	<i>0.037</i>	±0.005	0.120	<i>0.121</i>	±0.007	0.73	0.80	±0.08	0.032	<i>0.029</i>	±0.008	0.086	<i>0.092</i>	±0.010	0.76	0.79	±0.18
	48010911	9	0.049	<i>0.044</i>	±0.008	0.124	<i>0.127</i>	±0.011	0.76	0.83	±0.10	0.028	<i>0.029</i>	±0.011	0.079	<i>0.083</i>	±0.014	0.91	0.87	±0.17
HOBE	67013601	36	<b>0.030</b>	<b>0.035</b>	<b>±0.008</b>	<b>0.011</b>	<b>-0.004</b>	<b>±0.010</b>	<b>0.78</b>	<b>0.71</b>	<b>±0.13</b>	n/a	n/a	n/a	n/a	n/a	n/a	n/a	n/a	n/a
ALL SITES	AVERAGE	36	<b>0.040</b>	<b>0.035</b>	<b>±0.002</b>	<b>0.023</b>	<b>0.026</b>	<b>±0.003</b>	<b>0.66</b>	<b>0.74</b>	<b>±0.03</b>	<b>0.028</b>	<b>0.026</b>	<b>±0.003</b>	<b>-0.004</b>	<b>-0.007</b>	<b>±0.004</b>	<b>0.70</b>	<b>0.79</b>	<b>±0.06</b>
	AVERAGE	9	0.042	<i>0.038</i>	±0.002	0.043	<i>0.046</i>	±0.003	0.58	0.67	±0.03	0.032	<i>0.030</i>	±0.003	0.019	<i>0.009</i>	±0.004	0.56	0.70	±0.08

1141

1142 TABLE 4. Soil moisture metrics at individual reference pixels and (bottom two rows) averaged over 36-km and 9-km reference pixels.

1143 Information for 36-km reference pixels is shown in bold. Italics indicate L4\_SM metrics.



Site Name	Reference Pixel		Surface Soil Temperature (6am)									Surface Soil Temperature (6pm)								
	ID	Horiz. Scale [km]	ubRMSE [K]			Bias [K]			R [-]			ubRMSE [K]			Bias [K]			R [-]		
			NRv4	L4_SM Vv2030	95% Conf. Interval	NRv4	L4_SM Vv2030	95% Conf. Interval	NRv4	L4_SM Vv2030	95% Conf. Interval	NRv4	L4_SM Vv2030	95% Conf. Interval	NRv4	L4_SM Vv2030	95% Conf. Interval	NRv4	L4_SM Vv2030	95% Conf. Interval
REMEDHUS	03013602	36	2.0	1.5	±1.1	-4.0	-3.4	±1.3	0.98	0.99	±0.02	1.4	1.6	±1.1	-0.7	-2.1	±1.3	0.99	0.99	±0.02
	03010903	9	2.2	1.8	±1.2	-4.8	-4.2	±1.4	0.97	0.98	±0.03	1.6	2.0	±1.3	-1.8	-3.3	±1.5	0.99	0.99	±0.02
	03010908	9	1.7	1.2	±1.0	-3.8	-3.1	±1.1	0.98	0.99	±0.02	1.4	1.4	±1.2	-0.2	-1.6	±1.3	0.99	0.99	±0.03
Reynolds Creek	04013603	36	1.6	1.8	±1.9	-0.2	1.5	±1.9	0.98	0.98	±0.05	1.8	1.6	±1.7	2.5	0.9	±1.8	0.98	0.98	±0.04
	04010907	9	1.4	1.7	±1.6	0.3	2.2	±1.6	0.98	0.98	±0.04	1.7	1.5	±1.6	2.4	0.7	±1.7	0.98	0.98	±0.04
	04010910	9	2.5	2.5	±3.2	-2.5	-1.1	±3.1	0.96	0.96	±0.07	2.3	2.3	±2.7	0.1	-0.9	±2.7	0.96	0.96	±0.07
Yanco	07013601	36	1.8	1.5	±0.7	-3.5	-2.2	±0.8	0.97	0.98	±0.02	1.6	1.6	±0.6	0.7	-0.5	±0.8	0.98	0.98	±0.01
	07010902	9	1.9	1.4	±0.6	-3.1	-1.8	±0.8	0.97	0.98	±0.02	1.7	1.6	±0.5	1.6	0.3	±0.7	0.98	0.98	±0.02
	07010916	9	2.6	1.8	±0.8	-4.2	-2.9	±1.0	0.96	0.98	±0.03	1.7	1.6	±0.5	0.5	-0.8	±0.7	0.98	0.98	±0.02
Carman	09013610	36	2.6	2.6	±0.9	-3.1	-2.6	±1.2	0.93	0.93	±0.06	2.2	2.2	±0.9	1.4	0.3	±1.1	0.95	0.95	±0.05
	09010906	9	2.8	2.7	±1.0	-3.2	-2.8	±1.3	0.93	0.93	±0.07	2.3	2.2	±0.9	1.2	0.0	±1.2	0.95	0.95	±0.05
Ngari	12033601	36	2.4	2.0	±1.6	-5.2	-3.6	±1.9	0.90	0.92	±0.27	2.8	2.4	±0.8	-9.1	-12.5	±1.1	0.89	0.90	±0.12
Walnut Gulch	16013603	36	1.4	1.2	±0.5	-1.7	-1.5	±0.6	0.98	0.99	±0.02	1.6	1.7	±0.5	0.2	-2.1	±0.7	0.98	0.98	±0.02
	16010906	9	1.7	1.4	±0.6	-1.9	-1.7	±0.7	0.97	0.98	±0.02	1.9	1.9	±0.6	1.0	-1.5	±0.8	0.98	0.98	±0.02
	16010907	9	1.4	1.3	±0.6	-3.1	-2.8	±0.7	0.98	0.99	±0.02	1.7	1.7	±0.6	0.2	-2.2	±0.8	0.98	0.98	±0.02
	16010913	9	2.0	1.6	±1.5	-3.0	-2.6	±1.7	0.98	0.99	±0.06	2.1	2.3	±1.1	-0.3	-2.6	±1.4	0.98	0.98	±0.04
Little Washita	16023602	36	1.6	1.8	±1.0	-2.3	-1.7	±1.2	0.98	0.98	±0.02	1.8	1.8	±1.2	0.2	-0.5	±1.4	0.98	0.98	±0.02
	16020907	9	1.5	1.6	±1.0	-2.1	-1.5	±1.2	0.98	0.98	±0.02	1.7	1.7	±1.1	0.2	-0.6	±1.3	0.98	0.98	±0.03
Fort Cobb	16033602	36	1.5	1.5	±0.9	-2.3	-1.8	±1.0	0.98	0.99	±0.02	1.7	1.7	±0.9	0.3	-0.6	±1.1	0.98	0.98	±0.02
	16030911	9	1.3	1.3	±0.7	-1.8	-1.4	±0.9	0.99	0.99	±0.01	1.5	1.5	±0.9	0.4	-0.5	±1.1	0.99	0.99	±0.02
	16030916	9	1.4	1.5	±1.4	-1.7	-1.0	±1.5	0.97	0.98	±0.04	1.4	1.4	±1.4	0.8	0.0	±1.5	0.98	0.98	±0.05
Little River	16043602	36	1.5	1.5	±0.6	-3.0	-1.8	±0.8	0.98	0.99	±0.01	1.7	1.5	±0.7	-0.8	-1.7	±0.9	0.98	0.98	±0.02
	16040901	9	1.7	1.6	±0.6	-2.9	-1.8	±0.8	0.98	0.99	±0.01	1.8	1.7	±0.8	-1.1	-1.9	±1.0	0.98	0.98	±0.02
St Josephs	16060907	9	1.6	1.5	±0.9	-2.0	-1.3	±1.1	0.97	0.98	±0.02	1.6	1.5	±0.8	-0.2	-0.9	±1.0	0.98	0.98	±0.02
South Fork	16073602	36	1.6	1.6	±1.0	-2.3	-1.5	±1.1	0.98	0.98	±0.02	1.7	1.7	±1.1	-0.2	-0.9	±1.3	0.98	0.98	±0.02
	16070909	9	1.4	1.4	±0.7	-2.0	-1.2	±0.9	0.98	0.98	±0.02	1.5	1.5	±0.8	0.0	-0.6	±1.0	0.98	0.98	±0.02
	16070911	9	1.6	1.5	±0.8	-2.4	-1.7	±1.0	0.98	0.98	±0.02	1.6	1.6	±1.0	-0.3	-0.9	±1.2	0.98	0.98	±0.02
Monte Buey	19023601	36	1.2	1.2	±0.4	-2.6	-2.6	±0.5	0.97	0.97	±0.02	1.6	1.7	±0.5	-0.9	-1.9	±0.7	0.96	0.96	±0.03
	19020902	9	n/a	n/a	n/a	n/a	n/a	n/a	n/a	n/a	n/a	1.4	1.8	±0.7	0.3	-1.2	±0.8	0.97	0.94	±0.05
Tonzi Ranch	25013601	36	n/a	n/a	n/a	n/a	n/a	n/a	n/a	n/a	n/a	n/a	n/a	n/a	n/a	n/a	n/a	n/a	n/a	n/a
	25010911	9	n/a	n/a	n/a	n/a	n/a	n/a	n/a	n/a	n/a	n/a	n/a	n/a	n/a	n/a	n/a	n/a	n/a	n/a
Kenaston	27013601	36	1.3	1.4	±0.9	-1.5	-1.0	±1.0	0.98	0.97	±0.03	2.1	1.9	±1.2	1.5	0.5	±1.4	0.95	0.96	±0.05
	27010910	9	1.3	1.0	±0.6	-1.6	-1.1	±0.7	0.98	0.99	±0.02	1.8	1.5	±0.6	0.7	-0.3	±0.8	0.97	0.98	±0.03
	27010911	9	1.3	1.3	±0.9	-1.7	-1.2	±1.0	0.98	0.97	±0.03	2.1	1.8	±1.0	0.9	-0.1	±1.2	0.95	0.96	±0.04
Valencia	41010906	9	n/a	n/a	n/a	n/a	n/a	n/a	n/a	n/a	n/a	n/a	n/a	n/a	n/a	n/a	n/a	n/a	n/a	n/a
Niger	45013601	36	n/a	n/a	n/a	n/a	n/a	n/a	n/a	n/a	n/a	n/a	n/a	n/a	n/a	n/a	n/a	n/a	n/a	n/a
	45010902	9	n/a	n/a	n/a	n/a	n/a	n/a	n/a	n/a	n/a	n/a	n/a	n/a	n/a	n/a	n/a	n/a	n/a	n/a
Benin	45023601	36	n/a	n/a	n/a	n/a	n/a	n/a	n/a	n/a	n/a	n/a	n/a	n/a	n/a	n/a	n/a	n/a	n/a	n/a
	45020902	9	n/a	n/a	n/a	n/a	n/a	n/a	n/a	n/a	n/a	n/a	n/a	n/a	n/a	n/a	n/a	n/a	n/a	n/a
TxSON	48013601	36	1.1	1.1	±0.3	-2.0	-1.4	±0.4	0.99	0.99	±0.01	1.6	1.5	±0.6	-0.8	-1.8	±0.7	0.98	0.98	±0.02
	48010902	9	1.3	1.2	±0.4	-2.7	-2.2	±0.5	0.98	0.99	±0.01	1.8	1.7	±0.7	-1.6	-2.6	±0.9	0.98	0.98	±0.02
	48010911	9	1.3	1.2	±0.4	-2.3	-1.8	±0.5	0.98	0.99	±0.01	2.1	2.1	±0.8	-1.9	-2.9	±1.0	0.98	0.98	±0.02
HOBE	67013601	36	1.0	1.2	±0.5	-1.1	-0.4	±0.7	0.98	0.98	±0.02	1.1	1.2	±0.6	-0.8	-1.5	±0.8	0.98	0.98	±0.03
ALL SITES	AVERAGE	36	1.6	1.6	±0.2	-2.5	-1.7	±0.3	0.97	0.97	±0.01	1.8	1.7	±0.2	-0.5	-1.7	±0.3	0.97	0.97	±0.01
	AVERAGE	9	1.7	1.6	±0.3	-2.5	-1.8	±0.3	0.98	0.98	±0.01	1.8	1.7	±0.3	0.1	-1.1	±0.3	0.98	0.98	±0.01

1144

1145 TABLE 5. As in Table 4 but for soil temperature metrics.

1146

1147

1148

Sparse Network Subset	Surface Soil Moisture										Root Zone Soil Moisture									
	Number of sites	ubRMSE [ $m^3m^{-3}$ ]			Bias [ $m^3m^{-3}$ ]			R [-]			Number of sites	ubRMSE [ $m^3m^{-3}$ ]			Bias [ $m^3m^{-3}$ ]			R [-]		
		NRv4	<i>L4_SM</i>	95% Conf.	NRv4	<i>L4_SM</i>	95% Conf.	NRv4	<i>L4_SM</i>	95% Conf.		NRv4	<i>L4_SM</i>	95% Conf.	NRv4	<i>L4_SM</i>	95% Conf.	NRv4	<i>L4_SM</i>	95% Conf.
Forests (IGBP 1-5)	41	0.056	<i>0.054</i>	±0.005	0.104	<i>0.103</i>	±0.004	0.64	<i>0.65</i>	±0.03	34	0.047	<i>0.045</i>	±0.005	0.055	<i>0.055</i>	±0.005	0.62	<i>0.64</i>	±0.08
Open shrublands (IGBP 7)	27	0.037	<i>0.034</i>	±0.003	0.016	<i>0.030</i>	±0.003	0.66	<i>0.71</i>	±0.03	20	0.028	<i>0.026</i>	±0.005	-0.008	<i>0.006</i>	±0.004	0.66	<i>0.63</i>	±0.09
Woody savannas (IGBP 8)	28	0.065	<i>0.059</i>	±0.008	0.069	<i>0.060</i>	±0.006	0.65	<i>0.70</i>	±0.05	23	0.054	<i>0.048</i>	±0.010	0.037	<i>0.025</i>	±0.013	0.68	<i>0.70</i>	±0.13
Grasslands (IGBP 10)	177	0.053	<i>0.051</i>	±0.003	0.026	<i>0.031</i>	±0.003	0.65	<i>0.69</i>	±0.02	130	0.041	<i>0.042</i>	±0.006	-0.014	<i>-0.007</i>	±0.007	0.72	<i>0.69</i>	±0.07
Croplands (IGBP 12)	83	0.060	<i>0.057</i>	±0.003	0.026	<i>0.022</i>	±0.004	0.60	<i>0.64</i>	±0.03	60	0.046	<i>0.046</i>	±0.005	0.007	<i>0.004</i>	±0.005	0.65	<i>0.65</i>	±0.07
Urban/built-up (IGBP 13)	4	0.080	<i>0.071</i>	±0.017	0.027	<i>0.006</i>	±0.015	0.49	<i>0.62</i>	±0.11	3	0.047	<i>0.049</i>	±0.020	0.046	<i>0.032</i>	±0.019	0.64	<i>0.63</i>	±0.32
Crop/natural (IGBP 14)	39	0.060	<i>0.057</i>	±0.003	0.033	<i>0.027</i>	±0.003	0.66	<i>0.70</i>	±0.02	36	0.048	<i>0.045</i>	±0.003	0.008	<i>0.002</i>	±0.004	0.66	<i>0.69</i>	±0.06
Barren/sparse (IGBP 16)	2	0.033	<i>0.026</i>	±0.005	0.004	<i>0.016</i>	±0.004	0.61	<i>0.70</i>	±0.08	1	0.016	<i>0.017</i>	±0.020	-0.028	<i>-0.031</i>	±0.014	0.95	<i>0.92</i>	±0.35
Inside mask	279	0.056	<i>0.054</i>	±0.002	0.030	<i>0.028</i>	±0.002	0.64	<i>0.67</i>	±0.02	206	0.045	<i>0.044</i>	±0.003	-0.001	<i>-0.003</i>	±0.003	0.66	<i>0.66</i>	±0.04
Outside mask	127	0.052	<i>0.049</i>	±0.003	0.074	<i>0.078</i>	±0.002	0.64	<i>0.67</i>	±0.02	105	0.041	<i>0.040</i>	±0.004	0.040	<i>0.042</i>	±0.004	0.65	<i>0.65</i>	±0.05
<b>Average (all sites)</b>	<b>406</b>	<b>0.054</b>	<b><i>0.052</i></b>	<b>±0.002</b>	<b>0.050</b>	<b><i>0.051</i></b>	<b>±0.002</b>	<b>0.64</b>	<b><i>0.67</i></b>	<b>±0.01</b>	<b>311</b>	<b>0.044</b>	<b><i>0.042</i></b>	<b>±0.002</b>	<b>0.016</b>	<b><i>0.016</i></b>	<b>±0.003</b>	<b>0.66</b>	<b><i>0.66</i></b>	<b>±0.03</b>

1149

1150 TABLE 6. Sparse network metrics by land cover (IGBP class) and by the mask of the L4\_SM core validation site accuracy requirement

1151 (section 3c). Italics indicate L4\_SM metrics. Averages are based on a clustering algorithm (section 3c).

1152

1153 **Figure Captions**

1154

1155 Fig. 1. Schematic of the L4\_SM algorithm and data product. See section 2 for details and  
1156 abbreviations.

1157

1158 Fig. 2. (a) Surface soil moisture from (black solid line) L4\_SM Vv2030, (light blue solid line)  
1159 NRv4, and (red dots) *in situ* measurements at the 36-km Little Washita reference pixel  
1160 #16023602. (b) As in (a) but for root-zone soil moisture. See Table 4 for performance metrics.

1161

1162 Fig. 3. As in Figure 2 but for the 36-km Little River reference pixel #16043602.

1163

1164 Fig. 4. As in Figure 2 but for the 9-km South Fork reference pixel #16070911.

1165

1166 Fig. 5. (a) ubRMSE ( $\text{m}^3 \text{m}^{-3}$ ), (b) bias ( $\text{m}^3 \text{m}^{-3}$ ), and (c) R (dimensionless) for L4\_SM Vv2030  
1167 and NRv4 surface and root-zone soil moisture vs. core validation site measurements, averaged  
1168 across all 9-km and 36-km reference pixels. Error bars indicate 95% confidence intervals. The  
1169 thick horizontal line in panel (a) represents the L4\_SM accuracy requirement of  $\text{ubRMSE} \leq 0.04$   
1170  $\text{m}^3 \text{m}^{-3}$ .

1171

1172 Fig. 6. As in Figure 5 but for surface soil temperature at 6am and 6pm, with ubRMSE and bias  
1173 in K.

1174

1175 Fig. 7. ubRMSE ( $\text{m}^3 \text{m}^{-3}$ ) vs. sparse network measurements for L4\_SM Vv2030 (a,b) surface  
1176 and (c,d) root-zone soil moisture. (a,c) United States sites include (circles) SCAN, (inverted  
1177 triangles) USCRN, and (squares) OK Mesonet. (b,d) Australian sites are from OzNet. Gray  
1178 shading indicates areas with low or modest vegetation cover and topographic complexity that are  
1179 within the mask of the SMAP accuracy requirement (section 3c).

1180

1181 Fig. 8. As in Figure 7 but for the time series correlation coefficient R (dimensionless).

1182

1183

1184 Fig. 9. (a,b) ubRMSE ( $\text{m}^3 \text{m}^{-3}$ ), (c,d) bias ( $\text{m}^3 \text{m}^{-3}$ ), and (e,f) R (dimensionless) for L4\_SM  
1185 Vv2030 and NRv4 surface and root-zone soil moisture vs. sparse network measurements,  
1186 averaged across sites (a,c,e) within the mask and (b,d,f) outside the mask shown by the gray  
1187 shading in Figures 7 and 8. Averages are based on a clustering algorithm (section 3c). Error  
1188 bars indicate 95% confidence intervals.

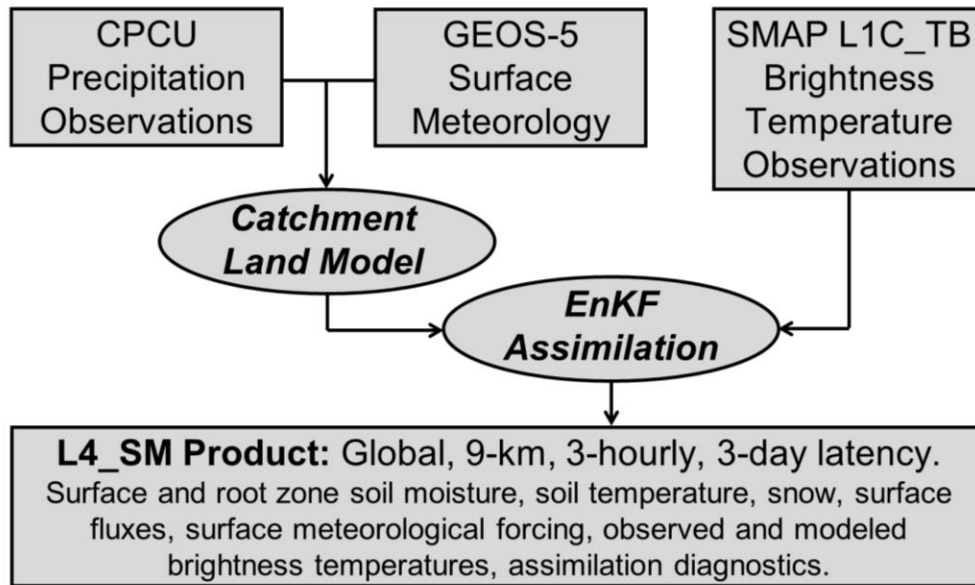
1189

1190

1191

1192 **Figures**

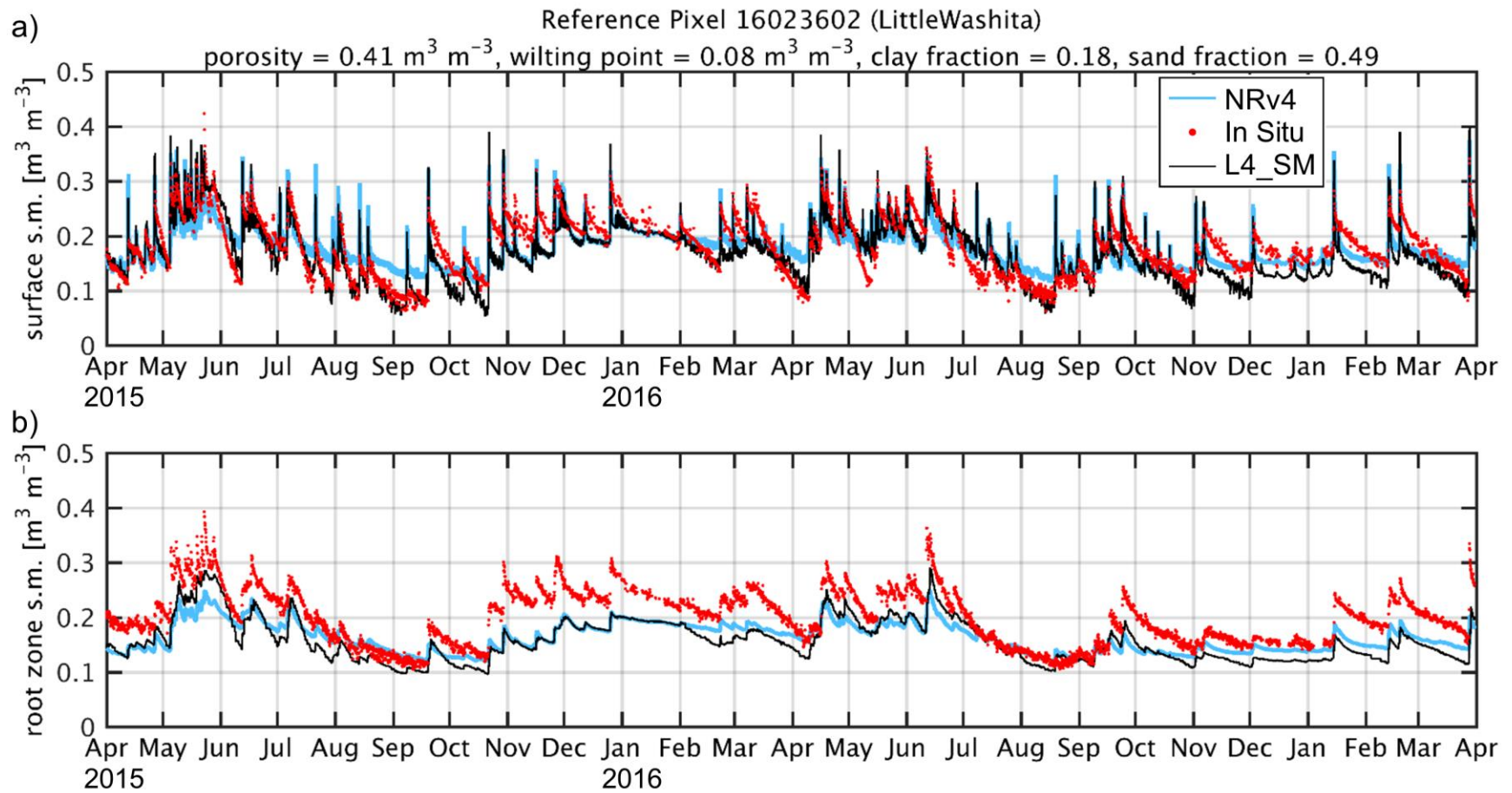
1193



1194

1195 Fig. 1. Schematic of the L4\_SM algorithm and data product. See section 2 for details and

1196 abbreviations.

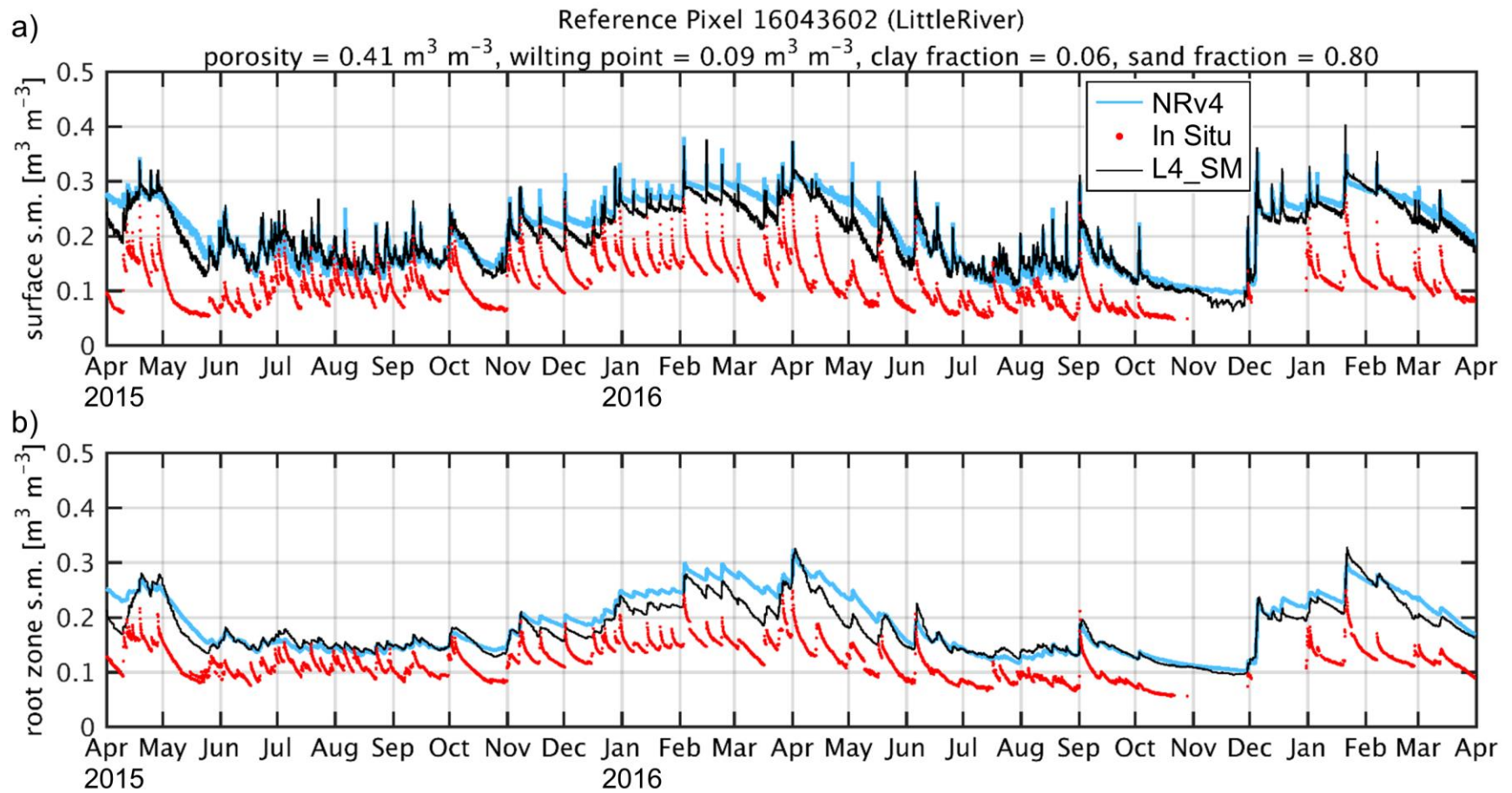


1197

1198 Fig. 2. (a) Surface soil moisture from (black solid line) L4\_SM Vv2030, (light blue solid line) NRv4, and (red dots) *in situ*

1199 measurements at the 36-km Little Washita reference pixel #16023602. (b) As in (a) but for root-zone soil moisture. See Table 4 for

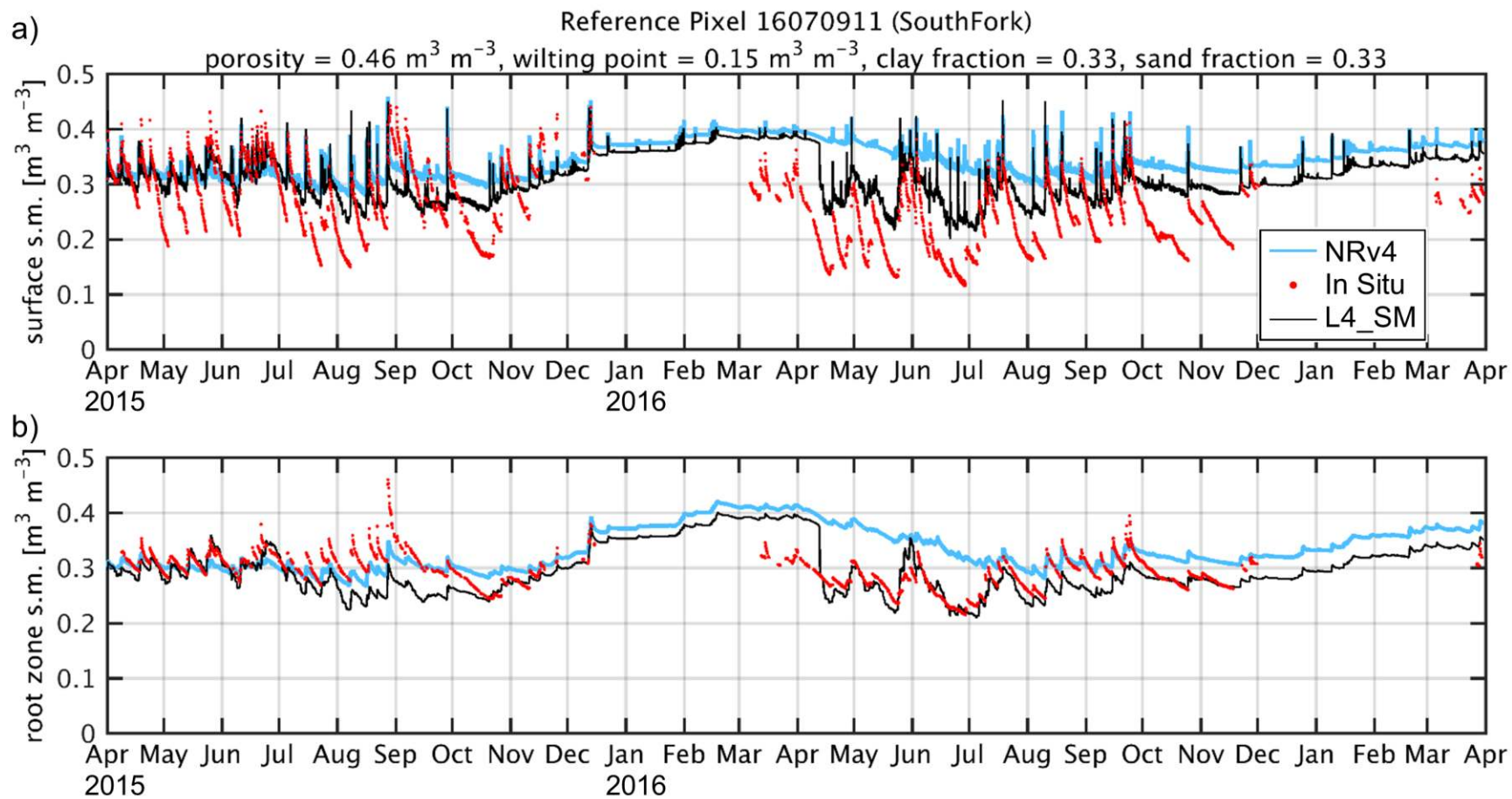
1200 performance metrics.



1201

1202 Fig. 3. As in Figure 2 but for the 36-km Little River reference pixel #16043602.

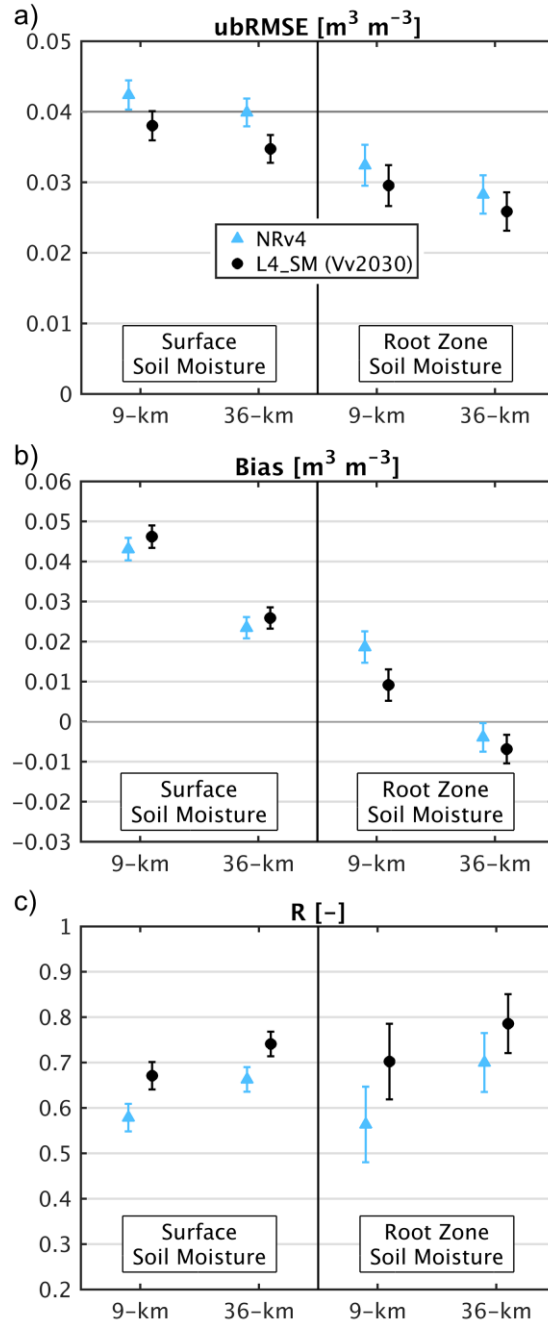
1203



1204

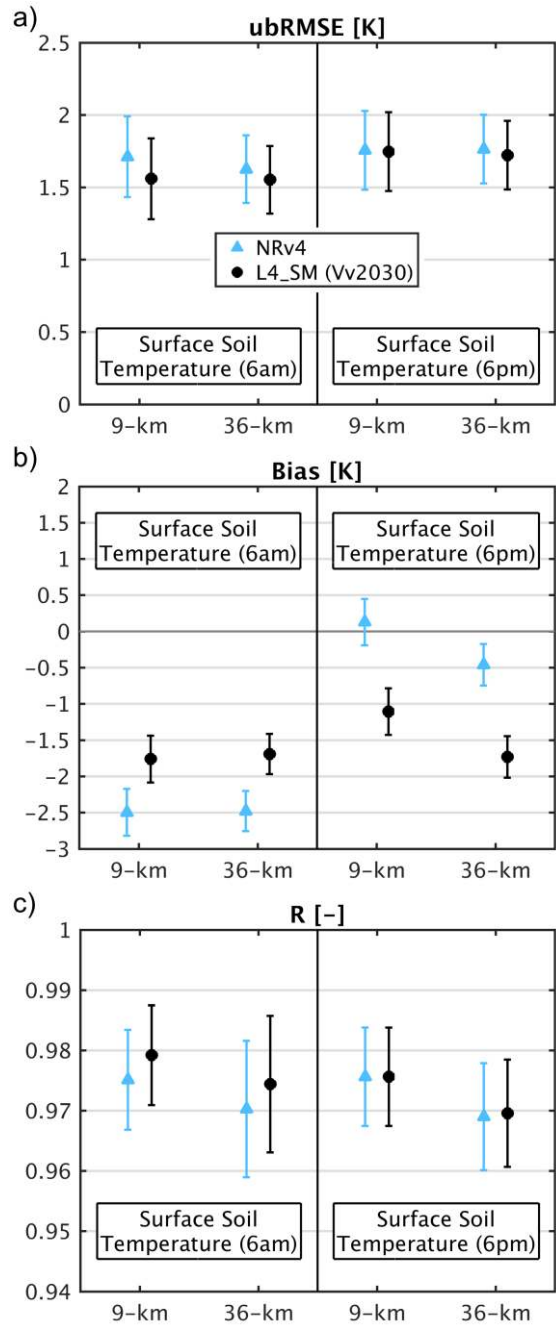
1205 Fig. 4. As in Figure 2 but for the 9-km South Fork reference pixel #16070911.





1206

1207 Fig. 5. (a) ubRMSE ( $\text{m}^3 \text{ m}^{-3}$ ), (b) bias ( $\text{m}^3 \text{ m}^{-3}$ ), and (c) R (dimensionless) for L4\_SM Vv2030  
 1208 and NRv4 surface and root-zone soil moisture vs. core validation site measurements, averaged  
 1209 across all 9-km and 36-km reference pixels. Error bars indicate 95% confidence intervals. The  
 1210 thick horizontal line in panel (a) represents the L4\_SM accuracy requirement of  $\text{ubRMSE} \leq 0.04$   
 1211  $\text{m}^3 \text{ m}^{-3}$ .

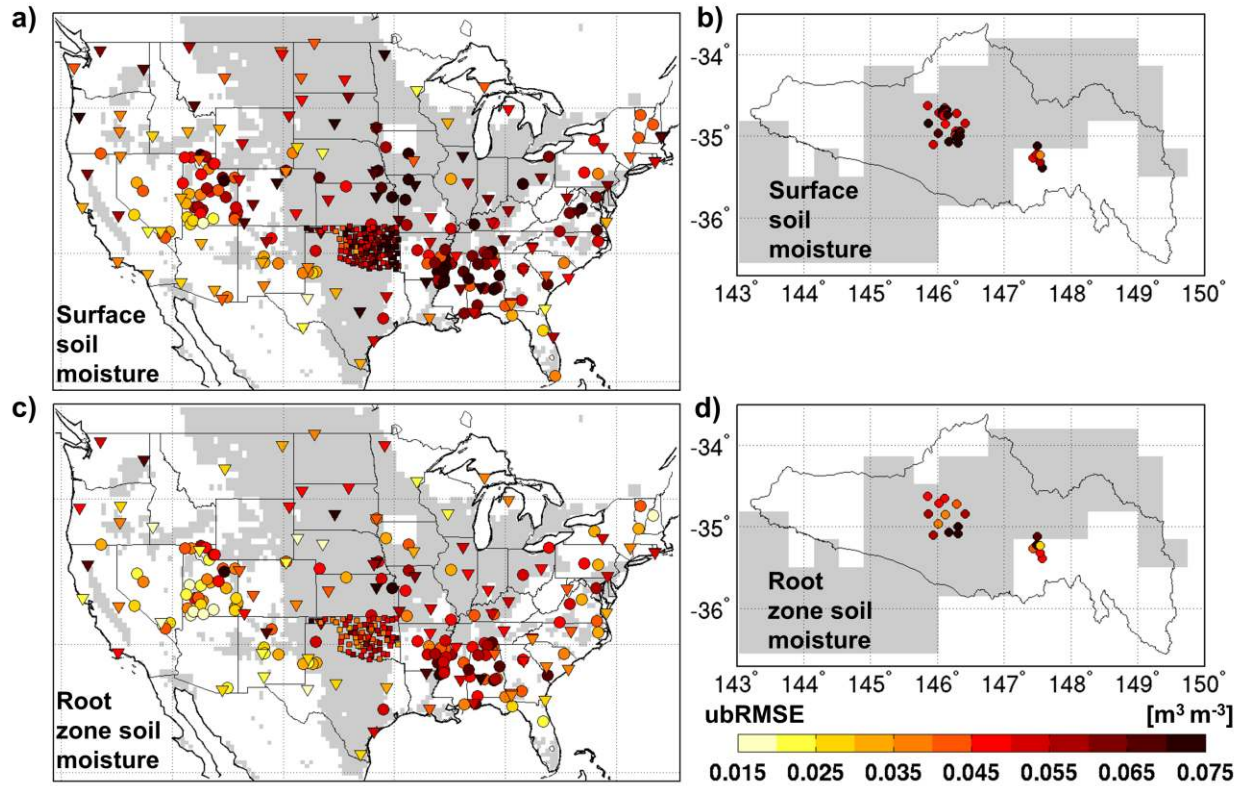


1212

1213 Fig. 6. As in Figure 5 but for surface soil temperature at 6am and 6pm, with ubRMSE and bias

1214 in K.

1215

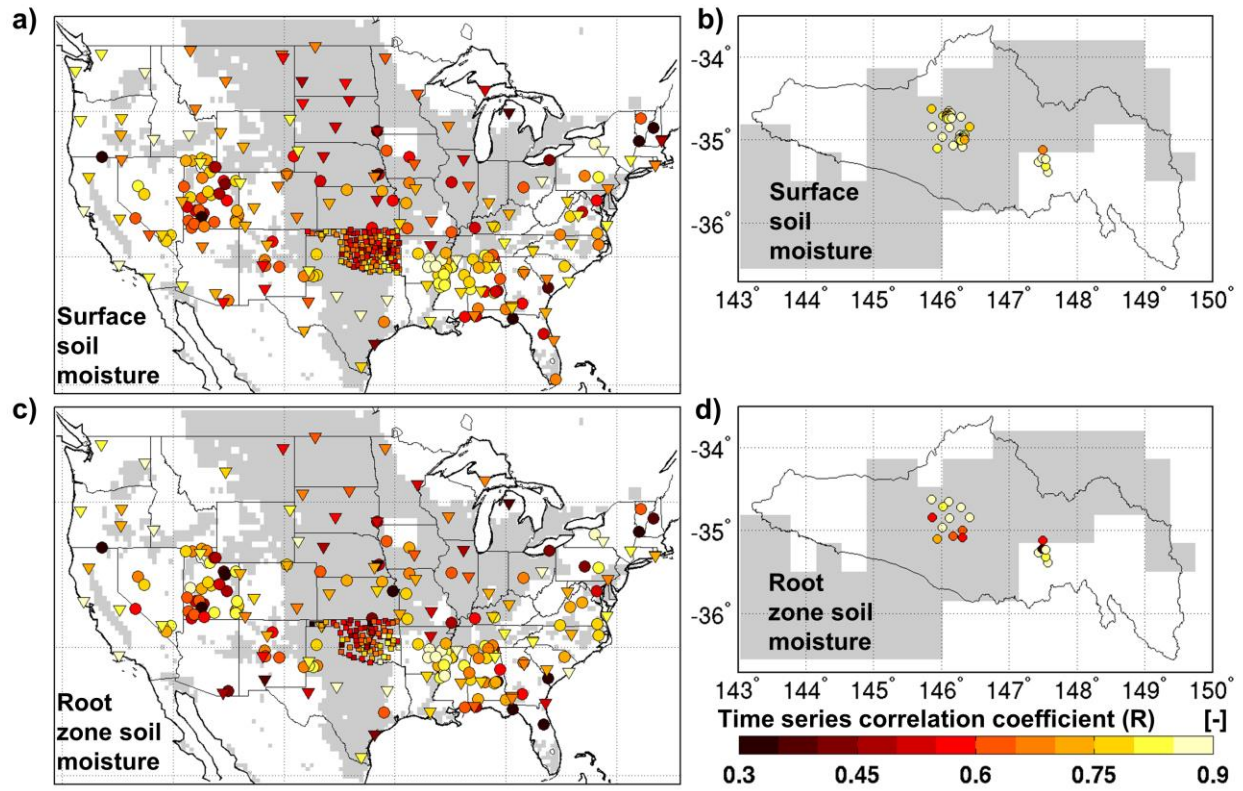


1216

1217 Fig. 7. ubRMSE ( $\text{m}^3 \text{m}^{-3}$ ) vs. sparse network measurements for L4\_SM Vv2030 (a,b) surface  
 1218 and (c,d) root-zone soil moisture. (a,c) United States sites include (circles) SCAN, (inverted  
 1219 triangles) USCRN, and (squares) OK Mesonet. (b,d) Australian sites are from OzNet. Gray  
 1220 shading indicates areas with low or modest vegetation cover and topographic complexity that are  
 1221 within the mask of the SMAP accuracy requirement (section 3c).

1222

1223



1224

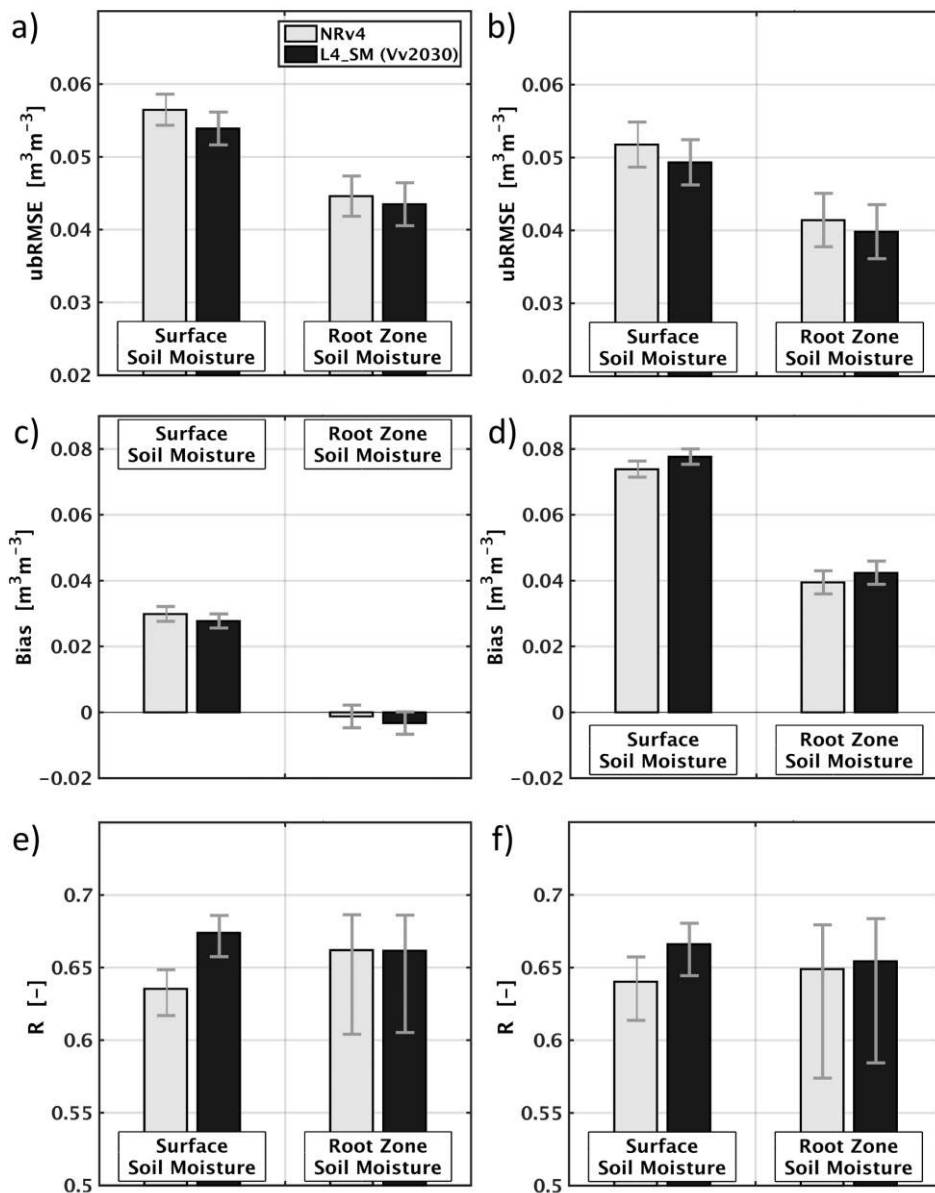
1225 Fig. 8. As in Figure 7 but for the time series correlation coefficient R (dimensionless).

1226

1227

Average across sites *not* located in mountainous topography, urban areas, and dense vegetation

Average across sites located in mountainous topography, urban areas, *or* dense vegetation



1228

1229 Fig. 9. (a,b) ubRMSE ( $\text{m}^3 \text{m}^{-3}$ ), (c,d) bias ( $\text{m}^3 \text{m}^{-3}$ ), and (e,f) R (dimensionless) for L4\_SM  
 1230 Vv2030 and NRv4 surface and root-zone soil moisture vs. sparse network measurements,  
 1231 averaged across sites (a,c,e) within the mask and (b,d,f) outside the mask shown by the gray  
 1232 shading in Figures 7 and 8. Averages are based on a clustering algorithm (section 3c). Error  
 1233 bars indicate 95% confidence intervals.